This discussion paper is/has been under review for the journal Atmospheric Chemistry and Physics (ACP). Please refer to the corresponding final paper in ACP if available.

The BLLAST field experiment: **Boundary-Layer Late Afternoon and** Sunset Turbulence

M. Lothon¹, F. Lohou¹, D. Pino^{2,23}, F. Couvreux³, E. R. Pardyjak⁴, J. Reuder⁵,

J. Vilà-Guerau de Arellano⁶, P. Durand¹, O. Hartogensis⁶, D. Legain³,

J. Vila-Guerau de Arellano^{*}, P. Durand^{*}, O. Hartogensis^{*}, D. Legam^{*}, P. Augustin⁷, B. Gioli¹⁵, I. Faloona⁸, C. Yagüe²¹, D. C. Alexander⁴, W. M. Angevine⁹, E. Bargain¹, J. Barrié³, E. Bazile³, Y. Bezombes¹, E. Blay-Carreras², A. van de Boer^{6,24}, J. L. Boichard¹⁰, A. Bourdon¹¹, A. Butet¹¹, B. Campistron¹, O. de Coster⁶, J. Cuxart¹², A. Dabas³, C. Darbieu¹, K. Deboudt⁷,

H. Delbarre⁷, S. Derrien¹, P. Flament⁷, M. Fourmentin⁷, A. Garai¹³, F. Gibert¹⁴, A. Graf¹⁶, J. Groebner¹⁷, F. Guichard³, M. A. Jimenez Cortes¹², M. Jonassen⁵, A. van den Kroonenberg¹⁸, D. H. Lenschow¹⁹, V. Magliulo²⁵, S. Martin²⁰, D. Martinez^{12,18}, L. Mastrorillo¹⁰, A. F. Moene⁶, F. Molinos¹², E. Moulin³, H. P. Pietersen⁶, B. Piguet³, E. Pique¹, C. Román-Cascón²¹, C. Rufin-Soler²²,

F. Saïd¹, M. Sastre-Marugán²¹, Y. Seity³, G. J. Steeneveld⁶, P. Toscano¹⁵, O. Traullé³, D. Tzanos³, S. Wacker¹⁷, N. Wildmann¹⁸, and A. Zaldei¹⁵

Received: 23 March 2014 - Accepted: 25 March 2014 - Published: 29 April 2014

Correspondence to: M. Lothon (marie.lothon@aero.obs-mip.fr)

Published by Copernicus Publications on behalf of the European Geosciences Union.

¹Laboratoire d'Aérologie, University of Toulouse, CNRS, France

²Applied Physics Department, Barcelona Tech UPC, Barcelona, Spain

³CNRM-GAME (UMR 3589, Météo-France and CNRS), Toulouse, France

⁴University of Utah, Salt Lake City, USA

⁵Geophysical Institute, University of Bergen, Bergen, Norway

⁶Meteorology and Air Quality Section, Wageningen University, Wageningen, the Netherlands ⁷Laboratoire de Physique et Chimie Atmosphériques, Université du Littoral Côte d'Opale, Dunkerque, France

⁸Land, Air and Water Resources, UC Davis, California, USA

⁹CIRES, University of Colorado, and NOAA ESRL, Boulder, Colorado, USA

¹⁰SEDOO, OMP, Toulouse, France

¹¹Service des Avions Français Instrumentés pour la Recherche en Environnement, CNRS-CNES-Météo-France, Francazal, France

12 Departament de Fisica, Universitat de les Illes Balears, Palma de Mallorca, Spain

¹³Mechanical and Aerospace Engineering, University of California, San Diego, California, USA

¹⁴Laboratoire de Météorologie Dynamique, Ecole Polytechnique, Palaiseau, France

¹⁵Institute of Biometeorology - National Research Council (IBIMET-CNR), Florence, Italy

¹⁶Institut für Bio- und Geowissenschaften, Juelich, Germany

¹⁷PMOD-WRC, Davos Dorf, Switzerland

¹⁸University of Tübingen, Tübingen, Germany

¹⁹National Center for Atmospheric Research, Boulder, Colorado, USA

²⁰Technische Universitaet Braunschweig, Braunschweig, Germany

²¹Dpt. Geofísica y Meteorología, Universidad Complutense de Madrid, Facultad Ciencias Físicas, Madrid, Spain

²²Institut de Recherches en ENvironnement Industriel (IRENI), Dunkerque, France

²³Institut of Space Studies of Catalonia (IEEC-UPC)

²⁴Meteorological Institute, University of Bonn, Bonn, Germany

²⁵Institute of Mediterranean Agricultural and Forest Systems – National Research Council (ISAFOM-CNR), Naples, Italy

Abstract

Due to the major role of the sun in heating the earth's surface, the atmospheric planetary boundary layer over land is inherently marked by a diurnal cycle. The afternoon transition, the period of the day that connects the daytime dry convective to the night-time stable boundary layer, still raises several scientific issues. This phase of the diurnal cycle is challenging from both modeling and observational perspectives: it is transitory, most of the forcings are small or null and the turbulence regime changes from fully convective regime, close to homogeneous and isotropic, toward a more heterogeneous and intermittent state.

These issues motivated the BLLAST (Boundary Layer Late Afternoon and Sunset Turbulence) field campaign that was conducted from 14 June to 8 July 2011 in southern France, in an area of complex and heterogeneous terrain. A wide range of integrated instrument platforms including full-size aircraft, remotely piloted aircraft systems (RPAS), remote sensing instruments, radiosoundings, tethered balloons, surface flux stations, and various meteorological towers were deployed over different surface types. The boundary layer, from the earth's surface to the free troposphere, was probed during the entire day, with a focus and intense observations from midday until sunset. The BLLAST field campaign also provided an opportunity to test innovative measurement systems, like new miniaturized sensors, and a new technique for frequent radiosoundings of the low troposphere.

Twelve fair weather days displaying various meteorological conditions were extensively documented during the field experiment. The boundary layer growth varied from one day to another depending on many contributions including stability, advection, subsidence, the state of the residual layer of the previous day, as well as local, meso- or synoptic scale conditions.

Ground-based measurements combined with tethered-balloon and airborne observations captured the turbulence decay from the surface throughout the whole boundary

10791

layer and evidenced the evolution of the turbulence characteristic lengthscales during the transition period.

Closely integrated with the field experiment, numerical studies are now underway with a complete hierarchy of models to support the data interpretation and improve the model representations.

1 Introduction

At interface between the earth's surface and the atmosphere, the planetary boundary layer (PBL) is a critical component of the earth system. It mediates the transfer of heat, momentum, humidity, and trace gases between the surface and the atmosphere.

The PBL over land has a strong diurnal cycle: on a fair weather day, as the sun rises, the surface heating warms the air above, which mixes by turbulent processes within an increasingly deep layer, engulfing air from the free atmosphere above (Stull, 1988; Garratt, 1992). Conversely during the night, the radiatively cooled surface stratifies the air above, which forms a stable nocturnal boundary layer. Both midday and nocturnal periods, when in a stationary state, have been relatively successfully modeled, even if several issues remain open (see the reviews by Angevine, 2008 and Holstlag et al., 2013). Morning and evening transitions remain difficult to observe and model, firstly due to their inherent transience. The late afternoon transition typically starts from a well-mixed convective boundary layer (CBL) and transforms to a residual layer overlying a stably-stratified surface layer. It has a lot of complexity, due to turbulence intermittency and enhancement of anisotropy, horizontal heterogeneity, rapidly changing conditions and combinations of weak forcing mechanisms.

The evolution of the PBL has been studied since the nineteen fifties. An extensive knowledge of the diurnal evolution of the PBL and its influence on the pollutant distribution has been gained since then (Vilà-Guerau de Arellano et al., 2004, 2009; Casso-Torralba et al., 2008). The increasing knowledge of PBL processes has been based on two main types of studies: the application of the theoretical concepts of tur-

bulence (Batchelor, 1967; Tennekes and Lumley, 1973; Pope, 2000; Wyngaard, 2010) to perform numerical simulations of the atmospheric characteristics (Lilly, 1967; Deardorff, 1972; Lenschow, 1974; Stull, 1976; Moeng, 1984; Jacobson, 2000; Pielke, 2002; Stensrud, 2007), and detailed field observations (e.g. Wangara 1967, Kansas 1968 or Minnesota 1973 (Hess et al., 1981; Kaimal and Wyngaard, 1990) remain fundamental references). There have been a large number of intensive field experiments since then, and in addition now, systematic observations made at some observatories allow to explore the PBL on a long-term basis as well, for example at Lindenberg, Germany (Beyrich and Engelbart, 2008), Cabauw, the Netherlands (Van Ulden and Wieringa, 1996; Hurley and Luhar, 2009; Baas et al., 2009; Bosveld et al., 2014) and Ciba, Spain (Yagüe and Cano, 1994), as well as flux monitoring networks worldwide.

Most PBL studies were previously devoted to investigating the PBL characteristics and the relevant processes during midday, when unstable or neutral conditions usually prevail (Kaimal et al., 1976; Mahrt and Lenschow, 1976; Stull, 1988; Moeng and Sullivan, 1994; Cuijpers and Holtslag, 1998), or at night when a stable atmosphere is typically found (Nieuwstadt, 1984; Debyshire, 1990; Garratt, 1992; Cuxart et al., 2000; Poulos et al., 2002; van de Wiel et al., 2003; Mahrt, 2014). Meteorological, air quality and global models have largely benefited from these investigations by introducing new process-based parameterizations.

As early as the late 1970s, though, André et al. (1978) compared a third order moment model with ground based measurements and soundings of the boundary layer during an entire diurnal cycle. Difficulties were found in the nocturnal conditions and during the late afternoon transition. Several recent studies have attempted to simulate the entire diurnal cycle both with large eddy simulation (LES) and single-column parametrized models (SCM). These include Kumar et al. (2006), Basu et al. (2008), or Svensson et al. (2011), who made use of realistic conditions based on the Horizontal Array Turbulence Study (HATS, Horst et al., 2004), Wangara campaign and CASES-99 respectively. Beare et al. (2006) and Edwards et al. (2006) compared surface observations at Cardington, UK with respectively a LES and a SCM from early afternoon to the

10793

next morning. The late afternoon transition decay was delayed in the LES relative to the observations, but a large improvement was found when assimilating the observations. The 1-D model had difficulties correctly representing turbulence diffusion during the afternoon transition, which affected the mean profiles. Most of the numerical simulations quoted above are able to reproduce the multi-layering that occurs in the evening and the generation of a nocturnal jet, but the transition timing remains hard to catch for several important variables (including surface fluxes, mean wind and temperature, and friction velocity). In addition, most of the simulations described above could only be compared with surface measurements of fluxes and turbulence and with vertical soundings of mean variables, but rarely with turbulence observations up to the PBL top.

There are still relatively few observational studies dedicated to transitory processes in the cloud-free or shallow convective atmospheric boundary layer; e.g. Grant (1997) (in Cardington, UK), Brazel et al. (2005) (Phoenix Air Flow Experiment), Fernando et al. (2004), Fernando et al. (2013a) (The Phoenix Evening Transition Flow Experiment). Also notable are the LIFT/FLATLAND experiment (Cohn et al., 2002) in the plains of Illinois, LITFASS (Beyrich et al., 2006) over heterogeneous surface in Germany, and CASES-99 (Poulos et al., 2002) in Kansas for the study of the nocturnal stable boundary layer. Without being specifically dedicated to the afternoon and evening transitions, these observational campaigns were the basis of key studies on the late afternoon or evening transitions.

The results based on the previously mentioned campaigns and on numerical experiments revealed some key issues of the late afternoon transition, which were chosen as the guideline for the Boundary layer Late Afternoon and Sunset Turbulence (BLLAST) project. In the following section, we present in more detail the issues raised by the afternoon transition, with the background of previous studies. Section 3 describes in detail the experimental set up and strategy that were chosen to address those issues, and Sect. 4 points out the potential of the BLLAST dataset.

2 Addressed issues

2.1 "Convective", "mixed" or "residual" layers? Definition and scaling

Definitions of the afternoon transition (AT) and the evening transition (ET) (and distinctions between them) may vary according to previous studies. Here, we adopt the same definitions as Nadeau et al. (2011): the AT starts as soon as the surface sensible heat flux begins to decrease and ends when it becomes negative. The ET is the period from the time of zero surface sensible heat flux to a well-established nocturnal stable layer, with quasi-steady depth. In the context of the AT and ET, the definitions of the surface layer, the mixed layer, the residual layer, and the nocturnal stable layer have to be carefully revisited. The late afternoon transition (LAT) corresponds to the later part of the AT, when the vertical structure starts to decouple (Grimsdell and Angevine, 2002) and the turbulence starts to decay.

Criteria typically used during midday to define the depth of the CBL are, among others: the depth of well-mixed scalars, depth of significant turbulence, the depth of increasing relative humidity, the depth from surface up to the capping inversion, or from the surface up to the point of minimum buoyancy flux (Angevine et al., 1994; Moeng and Sullivan, 1994; Seibert et al., 2000; Zhu and Albrecht, 2002; Brooks and Fowler, 2011). These criteria all find approximately the same depth in a well-defined CBL, but they start to evolve differently during the LAT and may separate from each other as observed e.g. by Grimsdell and Angevine (2002): the depth of the mixed layer may decrease, while the residual inversion remains level or evolves on its own notably depending on advection and subsidence.

In unstable conditions, the surface layer is mainly governed by shear and buoyancy, and the outer layer above is governed by buoyancy. Consequently, during the day, in convective conditions, most of the boundary layer processes in the outer layer can typically be scaled based on the surface buoyancy flux and the boundary-layer height (Deardorff scaling, Deardorff, 1970; Willis and Deadorff, 1976). In the surface layer, the Monin–Obukhov Similarity Theory (MOST, Monin and Obukhov, 1954) has been widely 10795

used. Both scalings are the basis for robust parameterizations in bulk and mesoscale models. However, during the afternoon transition, the surface buoyancy flux decreases toward zero, and the influence of other competing processes as radiation, advection, entrainment or wind shear become relatively more important. So neither the convective scaling, nor the stable boundary layer scaling, based on MOST as well, are valid. It is therefore necessary to explore the validity of convective and stable scalings, and how to represent the transition using non-dimensional analysis or new scalings. In this context, van Driel and Jonker (2011), based on an idealized LES and 0-D model study of a non-stationary PBL, suggest considering the time it takes for energy from the surface to reach the top of the boundary layer when defining a velocity scale. McNaughton et al. (2007), Sorbjan (2010, 2012), and Kumar et al. (2006) also proposed new scalings that could be tested in the context of transitory phases, like the local Richardson and Nieuwstadt local scalings.

2.2 Turbulence decay process

15 2.2.1 Turbulence kinetic energy (TKE) decay

Several authors have previously studied the transition regimes of turbulence with laboratory experiments (e.g. Cole and Fernando, 1993; Monin and Yaglom, 1975). The first LES study of the decaying atmospheric convective mixed layer was performed by Nieuwstadt and Brost (1986). The authors analyzed an academic case of a shearless, clear mixed layer, in which turbulence decayed as a result of a sudden shut-off of the upward surface heat flux. In both the LES simulations and the laboratory experiments, the turbulent kinetic energy is found to decay following a power law t^{-n} of time t.

Later, Sorbjan (1997) considered a gradual change of the heat flux with time, in response to the decreasing sun's elevation. The evolution of the decaying shearless mixed layer showed to be governed by two time scales: the external (or "forcing") time scale $\tau_{\rm f}$ – that is the time scale of the gradually changing of the heat flux – and the convective timescale $t_* = Z_{\rm i}/w_*$, where $Z_{\rm i}$ is the CBL depth, and w_* is the convective

velocity scale (Deardorff, 1970; Willis and Deardorff, 1976). In this context, the power coefficient n is a function of τ_f/t_* .

Recently, Nadeau et al. (2011) considered a realistic decrease of the surface sensible heat flux, based on observations of the LITFASS-2003 experiment (Beyrich and Mengelkamp, 2006). They showed that the TKE decay phase can be separated in two stages: first, a slow decay during the LAT followed by a rapid collapse of turbulence during the ET. Also Nadeau et al. (2011) were able to model the decay observed in the surface layer with a model based on a mixed-layer parameterization, rather than on a surface-based parameterization. Based on the CASES-99 dataset, Rizza et al. (2013) performed a LES study of the decay phase whose results corroborate the findings of Nadeau et al. (2011).

In both laboratory experiments and numerical studies like those mentioned above, the decay of the turbulent kinetic energy is found to depend on the formulation of the decrease in the surface—atmosphere energy exchanges (e.g. either expressed as prescribed surface sensible heat fluxes or surface temperature), but with no consensus on the exact relationship between the forcing and the power law.

On the observational side, Fitzjarrald et al. (2004) provided aircraft measurements of the turbulence decay within the PBL, and revealed a sharper and more systematic decay of the wind vertical velocity relative to the horizontal components. Most of the other previous observational studies have focused on the decay of the turbulent kinetic energy in the surface layer (e.g. Fernando et al., 2004; Brazel et al., 2005), with little quantification of how turbulence is decaying in the upper levels, and how the different levels interact with each other.

2.2.2 The evolution of length scales

²⁵ Characteristic scales of turbulence are relevant for understanding and quantifying PBL processes and their representation in meteorological models. Various length scales can be considered to characterize turbulence processes, with different ways to estimate them including: the wavelength of the energy spectrum peak (energy production), the

integral scale (energy-containing eddies) or other scales defined with a weighted integral of the spectrum, and also the buoyancy length scale, Ozmidov scale (Fernando, 1991), etc. During midday, those are often proportional (Lenschow and Stankov, 1986), but this is not expected to remain valid in the late afternoon.

Indeed, there is a lack of agreement in the evolution of the vertical velocity characteristic length scale during the late afternoon transition, partly due to the difficulty of addressing the issue, both with numerical studies and observations. Vertical motions up to 1 ms⁻¹ extending horizontally over several km have been observed, weaker but larger-scale than the midday eddies (Aupetit, 1989). Possible explanations for those include growth of boundary-layer scales, or surface variability and orography that can induce mesoscale circulations.

By using LES, Nieuwstadt and Brost (1986) found that the length scale of maximum spectral energy of the vertical velocity remained constant during the decay process. The study by Sorbjan (1997) mentioned previously reflected that small eddies had a tendency to decay earlier than large eddies. Consequently, organized convection persisted in the decaying mixed layer even when the buoyancy flux at the surface became negative, and a surface inversion was being developed near the earth's surface. These results were later confirmed by the direct numerical simulation of Shaw and Barnard (2002).

Pino et al. (2006) have shown that the characteristic length scale, based on a weighted integral of the density energy spectrum, have different evolution during the decay. They found that the characteristic length scale increases with time, for all variables but the vertical velocity, for which the scale remained almost constant. In contrast, based on tethered-balloon observations, Grant (1997) showed that the peak of the vertical velocity spectra shifts to smaller length scales during the ET.

With the TKE decay itself, the evolution of the characteristic length scales has been one of the main questions addressed in the past studies on the afternoon transition. However, the scale issue remains unclear and only partly understood. A thorough investigation of whether the scales in the mixed (and then residual) layer really increase

or decrease is necessary. In addition, it must be understood whether the characteristic length scales decrease in the surface layer as the nocturnal boundary layer starts to build, as stated by Kaimal and Finnigan (1994).

Another important related question is the anisotropy of the turbulence. Fitzjarrald et al. (2004) with flux towers and aircraft measurements and Pino et al. (2006) by means of LES, showed that the turbulence does not relax to an isotropic state during the decay process. Contrarily, Monin and Yaglom (1975) found in laboratory experiment that the turbulence maintains the initial isotropy during the decay. Lothon et al. (2006) have found with midday lidar observations in the CBL that the ratio between longitudinal (i.e. along the sampling direction) and transverse (i.e. perpendicular to the sampling direction) vertical velocity integral scales was smaller than it would be in isotropic turbulence, i.e. the turbulence is "squashed". However it remains unclear how squashed it remains later and until sunset.

2.2.3 Competing influences: "the unforced transition"

The decay of turbulence and the evolution of the characteristic length scales need to be related to the relevant forcing mechanisms, not only to the rate of surface buoyancy decrease, but also to competitive forces or processes generated by clouds, entrainment, radiative processes, shear and advection. Angevine (2008) suggests the term of "unforced transition", because those processes are usually weak during the LAT, but all may come into play.

The following questions are raised by the LAT:

15

- How does entrainment evolve during the AT? What is its role in the late afternoon transition? Nieuwstadt and Brost (1986) suggested that large eddies are still active for some time in driving entrainment at the top of the residual layer, in spite of the decoupling from the surface. This was corroborated numerically by Pino et al. (2006), but still needs to be confirmed by observations and further study. Canut et al. (2012) with a LES, found an increase of the entrainment rate in the

10799

late afternoon. The evolution of entrainment has to be linked to the evolution of scales. Van Heerwaarden et al. (2009) and Lohou et al. (2010) have shown how entrainment can have impact down to the surface, with signatures on evaporation or integral scales respectively. Thus, the evolution of the entrainment process needs to be linked with the evolution of lengthscales throughout the entire depth of the boundary layer.

- What is the influence of radiation in the decay process? Since the surface buoyancy flux is weak, the divergence of the radiative processes can make a significant contribution during this period, both at the surface and at the top of the mixed layer (Steeneveld et al., 2010).
- What is the role of land-use and surface heterogeneity in the evolution of turbulence intensity and scales? How do the heat storage in the ground or vegetation canopy and radiative long-wave and short-wave components come into play? Pardyjak and Fernando (2009) and Nadeau et al. (2011) have studied the turbulence decay in the surface layer over several types of surface and proposed a simple model for the decay in the convective surface layer. But the role of surface heterogeneity on the dynamics of the decaying mixed layer has still not been sufficiently addressed.
- How do the processes of the LAT interact with the flow reversal that occurs in mountainous or coastal areas, forced by mesoscale pressure and temperature gradients? Recently, the TRANSFLEX (The Phoenix Evening transition Flow Experiment, Fernando et al., 2013a), and MATERHORN (Fernando and Pardyjak, 2013b) addressed the issue of the flow reversal over mountain slopes during the evening transition. With tethered balloon observations and tracers along the slopes, Fernando et al. (2013a) showed the complexity of the flow adjustment, with the generation of multiple fronts in the flow reversal process. The LAT in complex terrain needs to be specifically addressed, since the LAT also precedes the shifting of a valley wind circulation, or sea breeze.

2.3 Potential impacts

Finally, the LAT may have important impacts on the transport, mixing and distribution of trace species, the set up of a nocturnal jet, or on the daytime growth of the following day.

– What is the impact of this transition on the transport of scalar species?

During the evening transition, Acevedo and Fitzjarrald (2001) reported occurrences of specific humidity jumps, and drops in surface temperature, accompanied by an abrupt decay in wind velocity. Similarly, Mahrt et al. (1999) observed that the latent heat flux during evening events decreased more slowly than the strength of turbulence and the boundary layer depth. This led to the significant moistening of the surface layer. This was also recently reported by Bonin et al. (2013) with unmanned aerial systems.

Recent studies (Vilà-Guerau de Arellano et al., 2004; Casso-Torralba et al., 2008) have shown that morning and afternoon transition are also important for the exchange of species. In early morning, when high entrainment rates have been observed, the remaining pollutants of the residual layer are introduced in the shallow boundary layer, thus increasing or decreasing their concentration. In the evening, the residual part overlying the stable layer can be incorporated in the free troposphere, so that water vapor and chemical components emitted at the surface and diluted into the convective layer during the day can be introduced in the free atmosphere and transported at larger scale, and in several layers (Banta et al., 1998; Berkowitz et al., 1998).

- How does the LAT interact with the appearance of the nocturnal jet?

Mahrt (1981, 1999) pointed out that the evolution of the stress divergence during evening transitions increased the ageostrophic flow, and led to the development of a low-level jet (wind speed maximum), accompanied by decoupling of the flow just above the surface.

The large number of studies originating from the CASES-97 and CASES-99 experiments (Poulos et al., 2002) provide a comprehensive documentation of the stable and 10801

very stable boundary layers and their turbulence regimes (van de Wiel et al., 2003; Sun et al., 2012), giving a better understanding of nocturnal drainage flows (Soler et al., 2002) and of the nocturnal jet (Banta et al., 2003), and proposing explanations for turbulence intermittency (van de Wiel et al., 2002a, b; Sun et al., 2003). CASES-99 also nicely documents the evening transition. Lundquist et al. (2003) for example revisited the explanations and occurrence of inertial oscillations. However, the role of the LAT in setting auspicious or unfavorable conditions for the appearance of the nocturnal jet and occurrence of turbulence intermittency still needs to be further addressed.

3 The BLLAST field experiment

The issues presented above motivated several research groups (listed in Table 1) to plan and execute a dedicated field experiment that focused on the afternoon and evening transitions, with a dense array of complementary observations in time and space from the mid-afternoon to the night.

The BLLAST field campaign took place in early summer, from 14 June to 8 July 2011 in France. The site is called "Plateau de Lannemezan", a plateau of about 200 km² area, a few km from the Pyreneean foothills (Fig. 1), and about 45 km from the Spanish border highest peaks. The surface is covered by heterogeneous vegetation: grasslands, meadows, crops and forest (Fig. 2). The campaign combined in situ measurements from towers, balloons and airplanes with ground-based remote sensing. The measurements were intensified during the LAT on days with favorable conditions (discussed later in the text), called Intensive Observation Periods (IOPs).

Two contrasted sites (hereafter "sites 1 and 2") contained most of the ground-based instruments and were the focus of flight operations. There were two main observational strategies, which focused on (1) vertical structure and (2) spatial heterogeneity. A third supporting site (site 3) was instrumented to allow the estimation of the 3-D wind circulation, advection terms and spatial variability at the sub-mesoscale.

In the following, we first describe the observations made continuously during the field experiment, and second those specifically made during the IOPs. The last subsections present the forecast models support during the field campaign, educational aspects, and the available dataset.

3.1 Continuous observations

3.1.1 Boundary-layer profiling

Several remote sensing instruments were deployed during BLLAST over the 3 sites for continuous monitoring of the atmosphere from 14 June to 8 July. Vertical profiling of the wind from 10 m to 16 kma.g.l. was accomplished at site 1 with a combination of sodar (from 10 m to 300 ma.g.l.), ultra-high frequency (UHF) radar (from 200 m to 3000 ma.g.l.) and very-high frequency (VHF) radar (from 1.5 km to 16 kma.g.l.) profilers. Both the UHF and the sodar profiling systems can also measure some characteristics of atmospheric turbulence (the turbulent energy dissipation rate can be estimated with a UHF profiler, and the temperature structure coefficient with a sodar). The UHF profiler also estimates the height of the mixed layer, or of any strong vertical gradients in the atmosphere (Angevine et al., 1994; Héo et al., 2003).

In addition, another UHF profiler and a sodar were deployed at sites 2 and 3, respectively (Fig. 1), to build a triangle of wind profilers, allowing to estimate the 3-D wind at the scale of the Plateau.

Lidars were also extensively utilized in the campaign. Two backscatter lidars, deployed at sites 1 and 2, monitored the aerosol vertical structure continuously during BLLAST. They provide estimations of the boundary layer top and depth of aerosol layers. A Doppler lidar was also operated at site 1, and provided profiles of wind vertical velocity at about 5 s time interval.

A ceilometer at site 1 supplied the cloud base height. A full sky camera was collocated with the ceilometer and provided a qualitative monitoring of the cloud cover with an image of the entire sky every minute.

10803

3.1.2 Surface layer measurements on various landscapes

During the BLLAST experiment, seven surface sites, hereafter denoted "ss1" to "ss7", were instrumented above various vegetation types and for different objectives (Figs. 2 and 3). The sites characteristics (altitude, vegetation type and height), the measured variables and the sensors used are listed in Tables A1 and A2 of the Appendix. In addition to classical meteorological measurements, all the sites had high-frequency sensors measuring turbulence properties. All eddy-covariance sensing systems were mounted at heights that ensure that the instruments were in the constant flux layer (above \sim 3–5 times the height of the local roughness elements), except the instruments mounted at the forest site where this was not possible. The first aim of those stations was to provide a thorough description of the surface fluxes in the heterogeneous land-scape of BLLAST area, while airborne and scintillometer measurements give access to integrated estimates. Beyond this, most of the surface stations were implemented with other dedicated objectives:

- At ss1 (on site 1) (Fig. 3a), two masts equipped with sensors for all surface energy components were installed in a grass and a wheat field respectively. A third station with a sonic anemometer and a fast water vapor and CO₂ sensor was located at the edge between both fields. Measurements from these stations are being used to investigate Monin Obukhov Similarity Theory over a heterogeneous terrain by using a flux-footprint model (van de Boer et al., 2013).
- The ss2 (at site 1) (Fig. 3d), was composed of two 10 m towers 20 m apart. The first tower was equipped with 6 sonic anemometers (at 0.85, 1.12, 2.23, 3.23, 5.27 and 8.22 m) and 9 fast-response fine-wire thermocouples (at 0.019, 0.131, 0.191, 0.569, 1.12, 2.23, 3.23, 5.27, 8.22 m). A second tower had 6 long-wave radiation sensors installed at the same heights as the sonics. The aim of this set-up was to investigate near-surface long-wave radiation and buoyancy flux divergence, and the delay between the surface flux sign change and the temperature gradient

sign change (Blay-Carreras et al., 2014b), as well as the formation of extremely shallow flows (Manins and Sawford, 1979; Mahrt et al., 2001).

- The ss3 (on site 1) (Fig. 3c) focused on a small-scale (a few meters) surface heterogeneity study (Cuxart et al., 2014). A flat surface (150 m × 150 m), covered with a mix of bare soil, small bushes, grass, and small puddles, which constituted a very heterogeneous surface, had its soil characteristics (temperature, humidity) extensively mapped. The vertical air temperature profile in the first 1.5 m and the energy fluxes were also monitored.

Three high-resolution microbarometers were also deployed at ss3, at each vertex of a triangle with 150 m side length, 1 ma.g.l. These high-precision digital instruments can detect very small pressure perturbations, in the order of 0.1 Pa, at 2 Hz sampling frequency. The objective was to study the small-scale static pressure fluctuations produced in the atmospheric boundary layer due to turbulent motions or the propagation of waves of different types (Viana et al., 2009, 2010; Sastre et al., 2012; Román et al., 2014).

- The ss4 is composed of the 60 m tower (Fig. 3d) which is a permanent platform at the Centre de Recherches Atmosphériques (CRA). It provides year-round flux-measurements and a vertical profile of turbulence close to surface. At the top of the tower, a high-resolution IR camera (1 Hz image frequency of a 45° x 34° field of view) pointed either toward the ss2, or toward the ss3 (Garai et al., 2013).
- At site 2, eddy-covariance stations sampled three contiguous large areas (about 1–2 km long) with relatively homogeneous vegetation: forest (ss5) (Fig. 3e), maize (ss6) and moor (ss7). The site was specifically devoted to the study of the role of surface heterogeneity. The turbulence characteristics and decay over the different vegetation covers will be compared taking into account the local circulations which may develop between the fields during this phase of the day.

10805

For consistency, a uniform data process was carried out for all eddy-covariance stations mentioned above.

In addition to the previous measurements, three scintillometers were used. They measured structure parameter of refractive index and temperature averaged along the path between the transmitter and the receiver (Moene et al., 2009). Therefore, and with the help of MOST theory, they provide an integrated measurement of surface fluxes over the heterogeneous regions sampled by the set of surface stations. A double beam laser scintillometer of 110 m path was deployed at ss1 (Hartogensis et al., 2002) and two large aperture scintillometers with path-lengths of 3 and 4 km toward the north and the south-east, respectively (Fig. 2).

Finally, for the purpose of characterizing aerosol optical properties and studying aerosol effects on the evolution of the boundary layer, aerosols size distribution was monitored at site 1, by use of a ground-based Scanning Mobility Particle Sizer (SMPS; range $10\,\text{nm}{-}1\,\mu\text{m})$ and an optical counter (OPC; range $0.3{-}20\,\mu\text{m}).$ For sulfates analysis, a proxy for secondary aerosols formation, aerosols were also collected at $12\,\text{m}$ height, using a three-stage cascade impactor, with cut-off diameters of $10\,\mu\text{m}$, $100\,\text{nm}$ and $30\,\text{nm}$.

3.2 Intensive observation periods (IOPs)

Observations were intensified under fair weather conditions, with mostly dry convection during the day, and clear sky or fair weather cumuli during the afternoon and evening transitions. These characteristics correspond to anti-cyclonic conditions (mountain-plain breeze regime), post-frontal conditions, or weak-pressure gradient conditions. These situations are not specific to the LAT study but typical for convective boundary-layer studies for which the influence of solar radiation on surface—atmosphere interaction plays a major role. Some IOP days were conducted the day following a rain episode when the morning was cloudy and conditions cleared up by midday. Over the 3.5 weeks of the field campaign, there were 12 days with favorable conditions (corresponding to 12 IOPs).

During the IOPs two manned aircraft, Remotely Piloted Aircraft Systems (RPAS), tethered and ascending balloons and in situ aerosol measurements were operated intensively. Figure 4 illustrates the observational strategy utilized during BLLAST IOPs and Table 2 summarizes the operation for each IOP.

For the joint operations of balloons, airplanes and RPAS, a Temporary Restricted Airspace (TRA) was issued and activated daily from 05:00 to 21:30 UTC. The TRA covered an area of 4 km radius including sites 1, 2 and 3 with an upper limit of 1.6 km a.g.l. (see Figs. 1 and 2). While activated, only the two manned BLLAST research aircraft were allowed to enter the TRA. In these cases all RPAS and tethered balloon operations were limited to low level flights, ensuring at least 150 m vertical separation between the lowest flight level of the manned aircraft and the highest of the RPAS.

3.2.1 Balloons

Radiosoundings

A total of 67 standard MODEM and GRAW radiosondes were launched from site 1 during the IOP days at least 4 times per day at 06:00, 12:00, 18:00, 24:00 UTC, and assimilated by the Météo-France forecast operational models (Table 2). At site 2, a new technique was used for frequent soundings of the lower troposphere only, during the AT (Legain et al., 2013). Two balloons, with different sizes, attached to the same Vaisala, were released. The larger balloon allowed ascent up to about 2 km height at which time the probe and the smaller balloon were separated from the larger balloon. The smaller balloon brought the probe safely to the ground. A package protecting the probe allowed its reuse after it was recovered. A real-time model predicted the landing area and aided in the decision of when to cut the line that released the probe and the smaller balloon. The time interval between two soundings was between 60 and 90 min. A total of 62 soundings were made with this technique, with 80 % probe retrieval rate (Table 2). Additionally, a few radiosondes were launched simultaneously at the three sites to estimate the divergence at the spatial scale of the plateau on IOPs 6, 7 and 11.

10807

Tethered balloons

Three tethered balloons (one at site 1 and two at site 2) operated during all the IOP days (except IOP 4, Table 2), from early afternoon to just after sunset. One balloon was equipped with a newly developed turbulence probe, operated at site 1 (Canut et al., 2014). This probe was composed of a sonic anemometer (Gill Windsonic 3-D), whose oscillations angles were measured by an inertial platform, and a platinum fine wire in a radiation shield for fast air temperature measurements. The probe was maintained at a given height, as fixed as possible, generally a few hundred meters above the ground, filling the gap of turbulence measurements between the 60 m tower and the lower leg of the aircraft, and giving a reference for the less validated RPAS measurements.

Two other tethered balloons, which measured mean meteorological variables (temperature, humidity, wind speed and direction), were operated at site 2, over the maize field and the moor field, with up to 5 probes at different heights, the four upper ones set at 2, 3, 5 and 9 m above the lowest one. The two tethered balloons were performing the same flight pattern: either they were maintained at a fixed low height (the probes were within 15 m height) or they profiled the first 150 m. The goal was to evaluate the impact of surface heterogeneity on the surface-layer vertical structure.

3.2.2 Aircraft

Two aircraft were chosen to participate in BLLAST (Fig. 5, top): the French Piper Aztec from SAFIRE (Saïd et al., 2005), and the Italian Sky Arrow from CNR (Gioli et al., 2006). The Sky Arrow participated from 14 June to 26 June, and the Piper Aztec stayed throughout the campaign (Table 2). Both aircraft measured pressure, temperature, moisture, $\rm CO_2$ concentration and 3-D wind with a spatial resolution of 1 m for the Sky arrow and around 3 m for the Piper Aztec. The detailed instrumentations of the Piper Aztec and the Sky Arrow are given in Tables A3 and A4 of the Appendix, respectively. The aircraft mainly flew in the middle-to-late afternoon. The flight plans were chosen to capture horizontal heterogeneity, vertical structure, the size of the turbulent

eddies size and their time evolution. Flights generally included stacked runs in vertical planes and helical profiles. In addition, simpler patterns such as flying a single track for a large number of passes to improve statistics were flown. The two aircraft flew either sequentially to entirely cover the time period from midday to after sunset; or, together during the same period in order to ensure improved spatial coverage and simultaneous measurements. The levels of particular horizontal flight legs depended on the boundary layer thickness, which was updated with UHF-radar or soundings from balloons or RPAS made before take off.

3.2.3 Remotely piloted aircraft systems

Table A5 of the Appendix lists the RPAS that flew, and acquired data of interest for BLLAST (see also Table 2 for the number of flights for the main RPAS used, and the picture in Fig. 5).

The small RPAS SUMO was mainly used for frequent profiling up to the top of the TRA and for low level (typically 60–80 m above ground) surface temperature mapping surveys (see an example in Fig. 6). Nearly 50 of the SUMO flights were performed with a newly integrated turbulence measurement system on board. It is based on a five-hole pressure probe and allows the determination of the 3-D flow vector approaching the aircraft with a frequency of 100 Hz (Reuder et al., 2012a, b).

M2AV (Martin et al., 2011) and MASC RPAS are suited for flying km-scale level legs with high-rate measurements of wind components, temperature and humidity fluctuations (van den Kroonenberg et al., 2012). Unfortunately, some technical problems occurred to the MASC, and no dataset could be supplied.

The other RPAS only participated during the last two weeks of the field campaign. These adjunct operations were performed as a RPAS test and sensor intercomparison event organized by the European COST Action ES0802 "Unmanned Aerial Systems in Atmospheric Research". In this context, the Octocopter operations were devoted to map the small-scale surface heterogeneities around the ss3 (Fig. 3e). SIRUS, BUSCA, Funjet 1 and 2 systems provided temperature and humidity data on non-IOP days.

10809

3.3 Forecasts

During the field campaign, specific forecast output was made available every hour, from two Numerical Weather Prediction (NWP) models of Météo-France: a global model, ARPEGE with a stretched horizontal resolution of about 10 km over France with a 4-

Dvar assimilation system, and a limited area non-hydrostatic model, AROME (Seity et al., 2011) with a standard resolution of 2.5 km. ARPEGE (Courtier et Geleyn, 1988) has about 11 levels within the first km (first level at 37 m), and AROME has about 15 levels (first level at 22 m).

There were two objectives in the AROME and ARPEGE forecast model output: (1) to help in the planning of the intensive observations during the field experiment, and (2) to evaluate the behavior of the two models, especially during the afternoon transition (Couvreux et al., 2014).

3.4 Educational aspects

Educational activities enabled undergraduate students from Germany and the Netherlands to participate in the field experiment thanks to the practical training programs of Bonn and Wageningen Universities that were integrated into the experimental plans. Additionally, several students also took a course on airborne atmospheric measurements and participated in BLLAST flights through the two associated EUFAR (European Facility for Airborne Research) projects BLLATE-1 and BLLATE-2. Several early stage researchers could participate in the campaign via the Short Term Scientific Mission (STSM) scheme provided by the COST Action ES0802.

3.5 Dataset

During the field experiment, a field catalog (http://boc.sedoo.fr) supplied quick looks of the continuous measurements and IOP observations, satellite images, reports, model forecasts and analyses, which are still available. The BLLAST web site (http:

//bllast.sedoo.fr) describes the project and contains the documentation, presentations and field catalog, and also gives access to the observational and modelling data and metadata. The dataset was reserved for BLLAST participants until spring 2014, and has been opened to the scientific community since then. We encourage people to con-

tact instrument Principal Investigators whenever using one of the BLLAST datasets.

4 Potential of BLLAST dataset

Here, we illustrate the potential of the observations made during the field experiment to address the issues raised by the LAT. We first show an overview of the conditions that were encountered during the field experiment, followed by a general description of some characteristics of the LAT, including the turbulence kinetic energy decay and the evolution of turbulence lengthscales.

4.1 Overview

Meteorological conditions

Figure 7 presents series of 24 h sequences for the 12 IOPs, from 14 June to 5 July 2011 of the solar irradiance, the wind speed and direction over the moor surface, the sensible heat flux over 6 different surfaces and at the top of the 60 m tower, and the evolution of Z_i (PBL depth) estimates from several sources and by the use of different criteria.

Contrary to the other days which were almost cloud-free, 14, 15, 24 and 30 June were partly cloudy (Fig. 7a), either with fair weather clouds, or starting with a stratocumulus cloud in the morning which broke into fair weather cumuli in the afternoon. Most of the time, those clouds were due to the rain and moisture advected into the area by frontal systems on previous days.

The wind at the surface was generally weak during the field campaign, with 10 min average values below 4 m s⁻¹ and daily averages < 2 m s⁻¹ for most of the IOPs (Fig. 7b). A typical nocturnal southerly downslope wind was frequently observed

(Fig. 7c) and, during the day, either north-easterly upslope winds (14, 15, 19, 20, 24 June and 1, 2 and 5 July, that are IOPs 0, 1, 2, 3, 4, 9, 10 and 11, respectively), or weak westerly winds on 30 June (IOP 8).

Surface sensible heat flux during the IOPs ranged between $100\,\mathrm{W\,m^{-2}}$ at midday over grass and moor and $400\,\mathrm{W\,m^{-2}}$ over the forest (Fig. 7d). At 60 m height, intermediate fluxes were measured, which is consistent with the fact that at this height, the flux resulted from contributions of several types of vegetated surfaces within the flux footprint area. The three IOPs 5, 6 and 7 (25–27 June) represent a particular period during the BLLAST experiment since they are characterized by a surface wind slightly higher than for the other IOPs (daily average of 3 ms⁻¹) and coming from the east. This less typical wind was due to the presence of a low pressure area in the lower troposphere over the Gulf of Lion in the Mediterranean Sea. Warm air occupied the entire troposphere, and led to very small sensible heat fluxes (Fig. 7d). Contrary to the sensible heat flux, the latent heat fluxes were much more similar between the various surfaces, reaching around 350 W m⁻² at midday for all IOPs and leading to different evaporative fraction values among the vegetation coverages (not shown).

Figure 7e shows an overview of the PBL growth during the IOPs over the entire field campaign. Estimates of Z_i were made from various observational sources, based on the following criteria: (C1) the height where the virtual potential temperature (θ_v) exceeds a certain threshold based on the value of θ_v at the surface, (C2) the height of maximum relative humidity, (C3) the height of maximum first derivative of the potential temperature, (C4) the height of minimum first derivative of specific humidity, (C5) the height of largest gradient of aerosol backscatter (from wavelet analysis), (C6) the height of maximum air refractive index structure coefficient (local maximum, with conditions on time continuity and consistency with the previous criterion). Criteria (C1), (C2), (C3) and (C4) were used for radiosonde and SUMO data, criterion (C5) for site 1 aerosol lidar data and criterium (C6) for site 1 UHF wind profiler data. Figure 7e only shows the criteria (C1) and (C2) for sounding and SUMO data, and criteria (C5) and (C6) for remote sensing. The results first show that the PBL was usually around 1000 m and

did not reach more than 1400 m over the campaign. It was particularly shallow during the hot period mentioned above on 25, 26 and 27 June. The morning growth rate was quite variable from day to day, but most of the time monotonic and smooth. The different estimates are in general consistent, but interestingly depart from each other on some specific days in the late afternoon. In those cases, the mixed layer depth detected from the thermodynamical criteria decreased with time in the late afternoon, while the residual top inversion and aerosol layer remained approximately the same (19, 24, 30 June and 1, 2, 5 July).

This overview shows the variety of conditions of fair weather encountered during the IOPs. The AT period as defined in Sect. 1 is indicated by the shaded areas for each day. Since it depends on each surface, the longest period is considered here: from the first time when the surface sensible heat flux is maximum on any surface, to the last time of its changing sign over any surface. It is interesting to see that the sensible heat flux may start to decrease (and the AT to start) before the downward radiation has reached its maximum (Fig. 7d), with still growing PBL for several hours before subsiding.

Also note that the sunrise is around 04:20 UTC during this period and at this area, and the sunset around 19:40 UTC.

4.1.2 Afternoon transition duration

Figure 8 quantifies the duration of the afternoon transition (AT) vs. the time at which the surface sensible heat flux starts to decrease, for all IOPs and several surface covers. Consistently with Grimsdell and Angevine (2002), we find that the AT can last several hours and have an early start. This is enhanced here by the singular hot period during IOPs 5, 6 and 7, which is characterized by the shortest AT durations (3 h), because the sensible heat flux changed its sign much earlier. Over grass and moor, characterized by larger evaporative fractions, the maximum of sensible heat flux can be reached early in the day, with AT durations spreading from about 3–4 h to about 7–8 h. In contrary, over forest and wheat, this maximum is normally reached around 12:00 UTC, and the AT lasts for about 6 h. Therefore, this figure shows how variable the start and the duration

of the AT can be according to the vegetation coverage and the meteorological conditions. The very early start (around 10:00 UTC) over some particular canopies even reveals the difficulty to correctly name this period. It is one aim of BLLAST to further address the role of the surface heterogeneity in the AT.

10813

Note that using buoyancy flux rather than sensible heat flux for the definition of the AT period does not change significantly the overall result. This is consistent with the larger differences found in sensible heat flux than in latent heat flux from one surface to the other (soil moisture is not a constraint during BLLAST). When the period is defined with buoyancy flux, the start time is delayed for 15 min in average and the time of zero flux is delayed of around 30 min in average, with more significant delay during the hot period.

4.1.3 Classification of the diurnal evolution of the PBL depth

The variety of forcings partly addressed in Sect. 2.2.3, including local processes, radiative forcing, large-scale subsidence and advection, etc., can lead to different PBL growth and evolution, according to the day.

Figure 9 shows the non-dimensional PBL growth of all IOP days, for comparison. The capping inversion of the convective boundary layer estimated by UHF radar or lidar is normalized here by the maximum height reached over the day. We found three ensembles for the 12 cases: (1) relatively typical cases with intermediate growth rates and a slightly descending summit inversion during the LAT (15, 20, 24, 25, 30 June, 2 July), (2) cases of rapid growth of the morning CBL, with levelling inversion during the LAT (14 June, 19 June and 1 July), (3) cases with slow growth of the CBL during the morning and rapid decrease of the inversion during the LAT (cases of 26 June, 27 June and 5 July). For the cases of the first "typical" class, the maximum of the depth of the CBL is reached within about 4 h from when the CBL begins to grow, while it is reached within about 1:30 min in the second class, and 5 or 6 h in the third class.

The evolution of the vertical structure observed in each of the three classes defined above is shown in more detail in Figs. 10 and 11, with three chosen examples.

Figure 10 shows a time-height cross-section of the TKE dissipation rate that is estimated from the UHF wind profiler Doppler spectral width (Jacoby-Koaly et al., 2002) for 24 June, 1 of July and 26 June, that are examples of the ensembles (1), (2) and (3) respectively. The capping inversion is superimposed. Figure 11 presents the vertical profiles of the potential temperature obtained from a selection of radiosoundings (standard radiosoundings or afternoon frequent radiosoundings) for the three same days. For the two first examples, Fig. 10 shows a decoupling during the LAT between the top of the mixed turbulent layer and the capping inversion. This is also consistent with observations by Grimsdell and Angevine (2002) and with Angevine (2008) stating that the decaying turbulent layer gets decoupled from the inversion as time goes by. We especially observe this for the typical ensemble (1) (Fig. 10a) and the rapid growth cases of ensemble (2) (Fig. 10b), with a decoupling between the turbulent layer and the summit inversion between 14:00 and 16:00 UTC, and a more rapid decay of the turbulent layer between 16:00 and 18:00 UTC. For the ensemble (3), a sharp decrease of the mixed turbulent layer is accompanied by a marked descent of the inversion in the first phase of the LAT.

The profiles in Fig. 11 show that for 1 July (Fig. 11b), the rapid growth of the morning CBL is due to the presence of a residual layer that remained close to neutral. This residual layer is well seen in the profile of 07:20 UTC, overlying the current mixed layer of 200 m depth. Once the mixing allowed the temperature to reach that of the residual layer above, the CBL depth rapidly integrated this residual layer in the mixed layer, as seen at 11:00 UTC. As shown in Fig. 10b, this day had significant turbulence (with also large TKE dissipation rates), and relatively deep CBL (Fig. 7e). The frequent radiosoundings reveal the presence of large-scale subsidence above the CBL top. Blay-Carreras et al. (2014a) have studied this case in detail, and especially analyzed the impact of the residual layer and of the presence of subsidence in the evolution of the CBL that day. During the LAT, the CBL keeps warming until 18:00 UTC with a slight descent of the CBL top. At 18:00 UTC, 1 h 40 min before sunset, the profile is still very

10815

well mixed but just beginning to stabilize. At 19:00 UTC, the temperature has decreased and the surface layer has started to stabilize.

The example of 26 June in Figs. 10c and 11c reveals a very limited growth of the CBL that hot day, with very light turbulence. The warmth of the entire troposphere during this period made it very difficult for the CBL to grow, with hardly any sensible heat flux at the surface. The decay of TKE dissipation rate is synchronized with the descent of the CBL top at the start of the LAT. Compared to 1 July, the stabilization of the surface layer has already started earlier at 17:00 UTC, as shown by the sounding in Fig. 11c.

The example of 24 June (Figs. 10a and 11a) for the more typical ensemble (1) presents several aspects similar to the 1 July, but with a less rapid growth of the CBL and smaller TKE dissipation rates. 25 June is studied in detail by Piertersen et al. (2014) and found as an example of "prototype" CBL.

This overview has shown the various types of boundary layers that were probed during BLLAST, which also depend on the mesoscale forcing. We have shown that the second class of rapid growth cases corresponds to cases with a well-established residual layer and a likely significant subsidence that prevents further growing of the CBL after its rapid morning rise. We have also identified a period of hot troposphere, which lead to very small sensible heat flux and large evaporative fraction, weak turbulence and poor CBL growth, that correspond to the third class.

The panel of various conditions shown in this subsection allowed us to define several so-called "golden days" (like 1 July, 25 June, 20 June, see Blay-Carreras et al., 2014a; Pietersen et al., 2014; Darbieu et al., 2014), which were selected to evaluate and compare to a complete hierarchy of numerical models, i.e.: forecast, mesoscale, and large-eddy simulation models (not addressed in this article – Jimenez et al., 2014; Angevine et al., 2014) or use one or the other model for a better understanding of some specific key processes.

4.2 Turbulence decay

Turbulence decay is one of the main foci of the analyses of BLLAST data. Here we give examples of this decay observed at the surface and in the boundary layer above and illustrate how BLLAST dataset enables to address the guestions raised in Sect. 2.2.1.

Figure 12 presents the turbulent kinetic energy decay observed from surface stations over 5 different surfaces and from aircraft, on all IOP days. RPAS and the turbulence probe carried by the tethered balloon at site 1 also measured turbulence at heights that are complementary to those probed by the aircraft and by the instrumented towers (not shown). So the BLLAST data set is expected to provide a diverse combination of estimates for the study of turbulence decay.

Figure 12 shows the two regimes of the decay that were presented by Nadeau et al. (2011): an initial slow decay (starting around 15:00 UTC in Fig. 12) followed by an abrupt decay (after 17:00 UTC). Based on this gradual afternoon decay, one can see the interest of considering the entire AT (which may start very early as we have seen before), when studying the LAT TKE decay, in order to start from the initial conditions of a fully convective and mixed boundary layer. The increase of TKE seen with surface measurements at the evening transition for some cases is due to the onset of the downslope valley wind after the mountain-plain circulation has reversed. Also note that the change of TKE with height is put into evidence by the varying flight levels and surface measurements, with larger TKE closer to the interfaces (surface and CBL top) than in the middle of the CBL.

The decay here is purposely shown with no scaling. The usual representation of the decay consists in a logarithmic diagram of the turbulence kinetic energy integrated over height (for LES studies especially) or observed at surface, divided by the square of the convective velocity scale at the initial time (midday) before the decay. Time is also normalized by the midday convective time scale (e.g. Sorbjan, 1997; Nadeau et al., 2011). That is, there is no effective normalization by a scaling factor that would evolve with time as the surface flux decreases. Using this usual technique with our dataset

10817

actually introduces more scattering in the measurements than what appears in Fig. 12, which motivated us not to use the midday Deardorff scaling in TKE and lengthscale representations in the present article.

The TKE decay process occurs throughout the whole depth of the boundary layer during the LAT as seen in Fig. 12. This general decay is consistent with the results of Nadeau et al. (2011) who were able to model the decay observed in the surface layer with a model that included mixed-layer parameters, rather than surface-based parameterization. It also supports the normalization proposed by van Driel and Jonker (2011).

However, a further combined observations-LES analysis of the time delay of the TKE decay according to the height should give clues about the way this decay propagates with height and on the evolution of forcings throughout the LAT. With the decrease of the surface fluxes and therefore the buoyancy, a decoupling should appear between the lower part of the still well mixed CBL and the upper part, within which the TKE starts to decrease. The TKE decay should then propagate from the CBL top down to the surface. This is further addressed by Darbieu et al., 2014 on a BLLAST case study. However, this is without considering strong shear and entrainment at the CBL top which might be able to partly maintain the TKE, increasing the relative contribution of the transport term in the TKE budget (as underlined by Grant, 1997). Preliminary analysis of the decay observed as a function of the synoptic conditions reveals the role that wind shear might play in delaying the abrupt decay phase (not shown), which supports the results found by Pino et al. (2006) with LES and by Goulart et al. (2010) with a theoretical model. The diversity of the conditions observed during BLLAST, together with measurements at different heights during the LAT, will allow a sensitivity analysis of the TKE decay with respect to the various forcing.

4.3 Evolution of integral scales

The BLLAST experiment can bring new insight on the turbulence scale evolution during the LAT by combining in situ measurements in the surface layer (from 2 to 60 m), in

situ high frequency measurements under tethered balloon at around 300 m height, a succession of aircraft flights from noon to sunset in the whole mixed layer and Doppler lidar vertical profiles of the vertical velocity.

Figure 13a shows the evolution of the integral scale $L_{\rm w}$ of the vertical wind velocity component during all IOPs, based on the Piper Aztec flights and on surface mea-

surements. The integral scale, which gives a characteristic eddy size, is estimated by integrating the vertical wind autocorrelation function from zero lag to the lag at which it drops to zero (Lenschow and Stankov, 1986). The wavelength of the maximum spectral energy is estimated by fitting the observed spectra with a simple analytical model of type $S(n) \propto \frac{1}{1+\frac{3}{2}(\frac{n}{n_0})^{5/3}}$, where S is the spectral energy density, n is the frequency and n_0 is the frequency of maximum energy. As expected, the integral scale increases with height: it is lower than 10 m near the surface and larger than 100 m in the mixed layer. Close to the surface, the integral scale decreases after 14:30 UTC, whereas it increases in the mixed layer slightly after 17:00 UTC. That is it varies little for a long part of the AT. This result partly agrees with Nieuwstadt and Brost (1986) or Pino et al. (2006) who pointed out a quite constant turbulence lengthscale of vertical velocity during the LAT, whereas the later sharper increase of the scale that we observe rather agrees with Grant (1997). However, it is important to note that the definitions of the turbulence lengthscales may differ from one study to the other, even if they should be proportional during convective conditions.

This is further illustrated in Fig. 13b, which shows the evolution of the ratio of the integral scale to the wavelength of the maximum spectral energy of the vertical velocity during all IOPs, based on the Piper Aztec flights and on surface measurements. This is an interesting way to normalize the integral scale, as it does not depend on Z_i , which becomes ambiguous when the turbulent mixed layer and the top inversion have decoupled. During midday, we find a ratio of about 0.35 at surface and about 0.15 within the CBL above, consistently with Lenschow and Stankov (1986) (see the profile in their Fig. 6). Interestingly, this ratio remains constant until 16:30 or 17:00 UTC – that is until the more abrupt phase of the TKE decay. Starting then, it decreases with time

10819

at surface imposed by a slower change in the integral scales than in the wavelength of the maximum spectral energy, and it increases above, in relation with a faster change in the integral scales than in the wavelength of the maximum spectral energy.

This raises the question of the possible decoupling with height of the turbulence processes during the LAT, that is addressed by Darbieu et al. (2014) who also study the evolution of the turbulence structure based on a spectral analysis of both LES and observations.

5 Conclusions

One of the main strengths of BLLAST project and field campaign is its focus on a well-defined issue: turbulence decay during the afternoon over land. Added to this, the large collaborative efforts that enabled assembling almost all the observational platforms that are useful for probing the PBL, as well as a complete hierarchy of modelling tools have resulted in a rich dataset for the study of the changing characteristics of turbulence during the LAT, throughout 12 IOP days. The field campaign took place in an environment of complex and heterogeneous terrain, which is both a challenge and an opportunity to link the LAT processes with mountain-plain flow reversal and surface heterogeneity.

The combination of manned and unmanned aircraft, together with numerous remote sensing systems and in situ techniques, each one with different capabilities, enable the interested community to (i) test and validate new sensors and techniques, (ii) gain a critical insight into (old and new) techniques through redundancy, and (iii) participate in the process studies of the LAT.

In particular, the frequent soundings of the atmosphere, with various techniques, have yielded a detailed description of the rapid evolution of the vertical structure of the lower troposphere. The numerous and complementary in situ and remote sensing observations of turbulence give an unprecedented exploration of turbulence decay during the LAT, and should enable us to make another step forward in the understanding and modelling of this process. Our preliminary analyses indicate that, in a broad sense, the

decay of TKE within the surface layer behaves quite similarly to that in the residual layer above. But further study of the temporal evolution of the different terms of the TKE budget at different levels is needed to verify how the decay varies with height, and what are the forcings, which control it. Contrary to the TKE, the turbulence integral scale highlights a more visible decoupling between the near surface layer and above with opposite trends in time, with a decrease of the turbulence scale near the surface and an increase above.

Closely integrated with the field experiment, numerical studies are currently underway with complementary types of models that enable us to further interpret the observations and test our hypotheses. Some of the numerical modelling and simulation activities include: (1) using forecast models (tested with BLLAST dataset in Couvreux et al., 2014) and mesoscale research models (Jimenez et al., 2014; Sastre et al., 2014; Angevine et al., 2014) to aid in understanding the large scale circulation and forcing within which the CBL develops, and for developing and testing parameterizations of the CBL; (2) using mixed layer models for understanding basic process-interactions and conceptualization of the questions raised (Pietersen et al., 2014; Blay-Carreras et al., 2014a); (3) using LES, which are able to resolve eddies down to a few meters (Pietersen et al., 2014; Darbieu et al., 2014; Blay-Carreras et al., 2014a), for better understanding the turbulence processes that we observe. Those three aspects should also help us to better understand the potential difficulties presented by the LAT for forecast or research models. BLLAST will thus contribute to the design of advanced high-resolution numerical simulations, by providing complementary data and allowing both more realistic simulations and a means to evaluate them.

Acknowledgements. The BLLAST field experiment was made possible thanks to the contribution of several institutions and supports: INSU-CNRS (Institut National des Sciences de l'Univers, Centre national de la Recherche Scientifique, LEFE-IMAGO program), Météo-France, Observatoire Midi-Pyrénées (University of Toulouse), EUFAR (EUropean Facility for Airborne Research) BLLATE-1&2, COST ES0802 (European Cooperation in the field of Scientific and Technical) and the Spanish MINECO projects CGL2009–08609, CGL2012–37416–C04–03, and CGL2011-13477-E. The field experiment would not have occurred without the contribution

10821

of all participating European and American research groups, which all have contributed in a significant amount. The Piper Aztec research airplane is operated by SAFIRE, which is a unit supported by INSU-CNRS, Météo-France and the French Spatial Agency (CNES). BLLAST field experiment was hosted by the instrumented site of Centre de Recherches Atmosphériques, Lannemezan, France (Observatoire Midi-Pyrénées, Laboratoire d'Aérologie). Its 60 m tower is partly supported by the POCTEFA/FLUXPYR European program. BLLAST data are managed by SEDOO, from Observatoire Midi-Pyrénées. See http://bllast.sedoo.fr for all contributions. Since 2013, the French ANR supports BLLAST analysis. Finally, we thank Harm J. J. Jonker, Robert J. Beare and Zbignew Sorbjan for fruitful discussions.

References

Acevedo, O. and Fitzjarrald, D. R.: The early evening surface-layer transition: temporal and spatial variability, J. Atmos. Sci., 58, 2650–2667, 2001.

André J.-C., De Moor, G., Lacarrère, P., Therry, G., and du Vachat, R.: Modeling the 24 h evolution of the mean and turbulent structures of the planetary boundary layer, J. Atmos. Sci., 78, 1861–1883, 1978.

Angevine, W. M.: Transitional, entraining, cloudy, and coastal boundary layers, Acta Geophys., 56. 2–20. 2008.

Angevine, W. M., White, A. B., and Avery, S. K.: Boundary-layer depth and entrainment zone characterization with a boundary-layer profiler, Bound.-Lay. Meteorol., 68, 375–385, 1994.

Angevine, W. M., Grimsdell, A. W., Hartten, L. M., and Delany, A. C.: The Flatland Boundary Layer Experiments, B. Am. Meteorol. Soc., 79, 419–431, 1998.

Angevine, W. M., Bazile, E., Legain, D., and Pino, D.: Land surface spinup for episodic modeling, Atmos. Chem. Phys. Discuss., 14, 4723–4744, doi:10.5194/acpd-14-4723-2014, 2014.

Aupetit, H.: Les Visiteurs du ciel Guide de l'air pour l'homme volant, 394 pp, Edition Rétine, Paris, France, 1989.

Baas, P., Bosveld, F. C., Baltink, H. K., and Holtslag, A. A. M.: A climatology of nocturnal low-level jets at Cabauw, J. Appl. Meteorol. Clim., 48, 1627–1642, 2009.

Banta, M., Senif, J., and Fehsenfeld, F. C.: Daytime buildup and nighttime transport of urban ozone in the boundary layer during a stagnation episode, J. Geophys. Res., 103, 22519–22544, 1998.

- Banta, R. M., Pichugina, Y. L., and Newsom, R. K.: Relationship between low-level jet properties and turbulence kinetic energy in the nocturnal stable boundary layer, J. Atmos. Sci., 60, 2549–2555, 2003.
- Basu, S., Vinuesa, J.-F., and Swift, A.: Dynamic LES modeling of a diurnal cycle, J. Appl. Meteorol. Clim., 47, 1156–1174, 2008.
 - Batchelor, G. K.: An Introduction to Fluid Mechanics, Cambridge University Press, London, 1967.
- Beare, R. J., Edwards, J. M., and Lapworth, A. J.: Simulation of the observed evening transition and nocturnal boundary layers: large-eddy modelling, Q. J. Roy. Meteor. Soc., 132, 81–99, 2006.
- Berkowitz, C. M., Fast, J. D., Springston, S. R., Larsen, R. J., Spicer, C. W., Doskey, P. VHubbe., J. M., and Plastridge, R.: Formation mechanisms and chemical characteristics of elevated photochemical layers over the northeast United States, J. Geophys. Res., 103, 10631–10647, 1998.
- Beyrich, F. and Engelbart, D. A. M.: Ten years of operational boundary-layer measurements at the Richard-Assmann Observatory Lindenberg: the role of remote sensing, 14th International Symposium for the Advancement of Boundary Layer Remote Sensing, 23–25 June 2008, Tech. Univ. of Denmark, Copenhagen, Denmark, 2008.
- Beyrich, F. and Mengelkamp, H.-T.: Evaporation over a heterogeneous land surface: EVA_GRIPS and the LITFASS-2003 Experiment an overview, Bound.-Lay. Meteorol., 121, 5–32, 2006.
- Blay-Carreras, E., Pino, D., Van de Boer, A., De Coster, O., Darbieu, C., Hartogensis, O., Lohou, F., Lothon, M., Pietersen, H., and Vilà-Guerau de Arellano, J.: Role of the residual layer and large-scale subsidence on the development and evolution of the convective boundary layer, Atmos. Chem. Phys. Discuss., 13, 31527–31562, doi:10.5194/acpd-13-31527-2013, 2013.
- Blay-Carreras, E., Pardyjak, E. R., Pino, D., Alexander, D. C., Lohou, F., and Lothon, M.: Countergradient heat flux observations during the evening transition period, Atmos. Chem. Phys. Discuss., 14, 7711–7737, doi:10.5194/acpd-14-7711-2014, 2014.
- Bonin, T., Chilson, P., Zielke, B., and Fedorovitch, E.: Observations of the early evening boundary-layer transition using a small unmanned aerial system, Bound.-Lay. Meteorol., 146, 119–132, 2013.

- Bosveld, F. C., Baas, P., van Meijgaard, E., de Bruijn, E. I.-F., Steeneveld, G.-J., and Holtslag, A. A. M.: The third GABLS intercomparison case for evaluation studies of boundary-layer models, Part A: Case selection and set-up, Bound.-Lay. Meteorol., doi:10.1007/s10546-014-9917-3, in press, 2014.
- Brazel, A. J., Fernando, H. J. S., Hunt, J. C. R., Selover, N., Hedquist, B. C., and Pardyjak, E. R.: Evening transition observations in Phoenix, Arizona, J. Appl. Meteorol., 44, 99–112, 2005.
 - Brooks, I. M. and Fowler, A. M.: An evaluation of boundary-layer depth, inversion and entrainment parameters by large-eddy simulation, Bound.-Lay. Meteorol., 142, 245–263, 2011.
- Canut, G., Couvreux, F., Lothon, M., Pino, D., and Saïd, F.: Observations and large-eddy simulations of entrainment in the Sheared Sahelian Boundary Layer, Bound.-Lay. Meteorol., 142, 79–101, 2012.
- Canut, G., Legain, D., Piguet, B., Moulin, E., and Tzanos, D.: The eddy-covariance method applied in a tethered-balloon, Atmos. Meas. Tech. Discuss., in preparation, 2014.
- Casso-Torralba, P. J., Vilà-Guerau de Arellano, J., Bosveld., F., Soler, M. R., Vermeulen, A., Werner, C., and Moors, E.: Diurnal and vertical variability of the sensible heat and carbon dioxide budgets in the atmospheric surface layer, J. Geophys. Res., 113, D12119, doi:10.1029/2007JD009583, 2008.
- Cohn, S. A., Mayor, S. D., Grund, C. J., Weckwerth, T. M., and Senff, C.: The Lidars in Flat Terrain (LIFT) Experiment, B. Am. Meteorol. Soc., 79, 1329–1343, 1998.
- Cole, G. and Fernando, H.: Some aspects of the decay of convective turbulence, Fluid Dyn. Res., 23, 161–176, 1998.
 - Courtier, P. and Geleyn, J.-F.: A global numerical weather prediction model with variable resolution application to the shallow-water equations, Q. J. Roy. Meteor. Soc., 114, 1321–1346, 1988.
- Couvreux, F., Bazile, E., Seity, Y., Lothon, M., Guichard, F., Canut, G., Lohou, F., Pietersen, H., and Legain, D.: Representation of the afternoon transition in Numerical Weather Prediction models: evaluation with BLLAST dataset, Atmos. Chem. Phys. Discuss., in preparation, 2014.
 - Cuijpers, J. W. M. and Holtslag, A. A. M.: Impact of skewness and nonlocal effects on scalar and buoyancy fluxes in convective boundary layers, J. Atmos. Sci., 55, 151–162, 1998.
 - Cuxart, J., Yagüe C., Morales, G., Terradellas, E., Orbe, J., Calvo, J., Fernández A., Soler, M. R., Infante, C., Buenestado, P., Espinalt, A., Joergensen, H. E., Rees, J. M., Vilà-Guerau de Arellano, J., Redondo, J. M., Cantalapiedra, I. R., and Conangla, L.: Stable Atmospheric

- Boundary-Layer Experiment in Spain (SABLES 98): a report, Bound.-Lay. Meteorol., 96, 337-370, 2000.
- Cuxart, J., Wrenger, B., Duennermann, J., Martinez, D., Jimenez, M. A., Conangla, L., Reuder, J., Jonassen, M. O., Lothon, M., Saïd, F., and Lohou, F.: Sub-kilometric heterogeneity effects on the surface energy budget in BLLAST'11, Atmos. Chem. Phys. Discuss., in preparation, 2014.
- Darbieu, C., Lohou, F., Lothon, Vilà-Guerau de Arellano, J., Durand, P., Blay, E., Pino, D.: Turbulence vertical structure of the boundary layer during the late afternoon transition, Atmos. Chem. Phys. Discuss., in preparation, 2014.
- Deardorff, J. W.: Convective velocity and temperature scales for the unstable planetary boundary layer and for Rayleigh convection, J. Atmos. Sci., 27, 1211–1215, 1970.
 - Deardorff, J. W.: Numerical investigation of neutral and unstable planetary boundary layers, J. Atmos. Sci., 29, 91–115, 1972.
 - Derbyshire, S. H.: Nieuwstadt's stable boundary layer revisited, Q. J. Roy. Meteor. Soc., 116, 127–158, 1990.
 - Edwards, J. M., Beare, R. J., and Lapworth, A. J.: Simulation of the observed evening transition and nocturnal boundary layers: single column modelling, Q. J. Roy. Meteor. Soc., 132, 61–80, 2006.
 - Fernando, H. J. S.: Turbulent mixing in stratified fluids, Annu. Rev. Fluid Mech., 23, 455–493, 1991.
 - Fernando, H. J. S. and Pardyjak, E. R.: Field studies delve into the intricacies of mountain weather, Eos, Transactions American Geophysical Union, 94, 313–315, 2013.
 - Fernando, H. J. S., Princevac, M., Pardyjak, E., and Data, A.: The decay of convective turbulence during evening transition period, in: Proc. of the 11th Conference on Mountain Meteorology and MAP Meeting, Bartlett (NH), USA, 2004.
 - Fernando, H. J. S., Verhoef, B., Di Sabatino, S., Leo, L. S., and Park, S.: The Phoenix Evening Transition Flow Experiment (TRANSFLEX), Bound.-Lay. Meteorol., 147, 443–468, 2013.
 - Fitzjarrald, D. R., Freedman, J. M., Czikowsky, M. J., Sakai, R. K., Acevedo, O. C., and Moraes, O. L. L.: Momentum and scalar transport during the decay of CBL turbulence, in: Proc. 16th AMS Symposium on Boundary Layers and Turbulence, 9–13 August 2004, Portland (ME), USA, 2004.
 - Garai, A., Pardyjak, E., Steeneveld, G.-J., and Kleissl, J.: Surface temperature and surface-layer turbulence in a convective boundary layer, Bound.-Lay. Meteorol., 148, 51–72, 2013.

- Garratt, J. R.: The Atmospheric Boundary Layer, Cambridge University Press, 316 pp., 1992.Gioli, B., Miglietta, F., Vaccari, F. P., Zaldei, A., and De Martino, B.: The Sky Arrow ERA, an innovative airborne platform to monitor mass, momentum and energy exchange of ecosystems, Ann. Geophys., 49, 109–116, 2006,
- http://www.ann-geophys.net/49/109/2006/.
 - Goulart, A. G., Bodmann, B. E. J., Vilhena, M. T. M. B., Soares, P. M. M., and Moreira, D. M.: On the time evolution of the turbulent kinetic energy spectrum for decaying turbulence in the convective boundary layer, Bound.-Lay. Meteorol., 138, 61–75, 2010.
- Grant, A. L. M.: An observational study of the evening transition boundary-layer, Q. J. Roy. Meteor. Soc., 123, 657–677, 1997.
- Grimsdell, A. W. and Angevine, W. M.: Observations of the afternoon transition of the convective boundary layer, J. Appl. Meteorol., 41, 3–11, 2002.
- Hartogensis, O. K., De Bruin, H. A. R., and van de Wiel, B. J. H.: Displaced-beam small aperture scintillometer test, Part II: CASES-99 stable boundary-layer experiment, Bound.-Lay. Meteorol., 105, 149–176, 2002.
- Heo, B.-H., Jacoby-Koaly, S., Kim, K. E., Campistron, B., Benech, B., and Jung, E.-S.: Use of the Doppler spectral width to improve the estimation of the convective boundary layer height from UHF Wind Profiler Observations, J. Atmos. Ocean. Tech., 20, 408–424, 2003.
- Hess, G., Hicks, B., and Tetsuji, Y.: The impact of the Wangara experiment, Bound.-Lay. Meteorol., 20, 135–174, 1981.
- Holtslag, A. A. M., Svensson, G., Baas, P., Basu, S., Beare, R., Beljaa rs, A. C. M., Bosveld, F. C., Cuxart, J., Lindvall, L., Steeneveld, G. J., Tjernström, M., and Van De Wiel, B. J. H.: Stable atmospheric boundary layers and diurnal cycles: challenges for weather and climate models, B. Am. Meteorol. Soc., 94, 1691–1706, 2013.
- Horst, T. W., Kleissl, J. Lenschow, D. H., Meneveau, C., Moeng, C.-H., Parlange, M. B., Sullivan, P. P., and Weil, J. C.: HATS: field observations to obtain spatially filtered turbulence fields from crosswind arrays of sonic anemometers in the atmospheric surface layer, J. Atmos. Sci., 61, 1566–1581, 2004.
 - Hurley, P. and Luhar, A.: Modelling the meteorology at the Cabauw tower for 2005, Bound.-Lay. Meteorol., 132, 43–57, 2009.
 - Jacobson, M. Z.: Fundamentals of Atmospheric Modeling, Cambridge University Press, 666 pp., 2000.

- Jacoby-Koaly, S., Campistron, B., Bernard, S., Benech, B., Girard-Ardhuin, F., Dessens, J., Dupont, E., and Carissimo, B.: Turbulent dissipation rate in the boundary layer via UHF wind profiler Doppler spectral width measurements, Bound.-Lay. Meteorol., 103, 361–389, 2002.
- Jimenez, M. A., Angevine, W. M., Bazile, E., Couvreux, F., Cuxart, J., Pino, D., and Sastre, M.: An intercomparison of mesoscale simulations during the Boundary Layer Late Afternoon and Sunset Turbulence (BLLAST) experimental field campaign, Atmos. Chem. Phys. Discuss., in preparation, 2014.
- Kaimal, J. C. and Finnigan, J. J.: Atmospheric Boundary Layer Flows Their Structure and Measurement, Oxford University press, 289 pp., 1994.
- Kaimal, J. and Wyngaard, J.: The Kansas and Minnesota experiments, Bound.-Lay. Meteorol., 50, 31–47, 1990.
 - Kaimal, J. C., Wyngaard, J. C., Haugen, D. A., Coté O. R., Izumi, Y., Caughey, S. J., and Readings, C. J.: Turbulence structure in the convective boundary layer, J. Atmos. Sci., 33, 2152–2169, 1976.
- Kumar, V., Kleissl, J., Meneveau, C., and Parlange, M. B.: Large-eddy simulation of a diurnal cycle of the atmospheric boundary layer: atmospheric stability and scaling issues, Water Resour. Res., 42, 3–18, 2006.
 - Legain, D., Bousquet, O., Douffet, T., Tzanos, D., Moulin, E., Barrie, J., and Renard, J.-B.: High-frequency boundary layer profiling with reusable radiosondes, Atmos. Meas. Tech., 6, 2195–2205, doi:10.5194/amt-6-2195-2013, 2013.
 - Lenschow, D. H.: Model of the height variation of the turbulence kinetic energy budget in the unstable planetary boundary layer, J. Atmos. Sci., 31, 465–474, 1974.
 - Lenschow, D. H. and Stankov, B. B.: Length scales in the convective boundary layer, J. Atmos. Sci., 43, 1198–1209, 1986.
- Lilly, D. K.: The Representation of Small-Scale Turbulence in Numerical Simulation Experiments, Proc. of IBM Scientific Computing Symposium on Environmental Sciences, Yorktown Heights, USA, 1967.
 - Lohou, F., Saïd, F., Lothon, M., Durand, P., and Serça, D.: Impact of boundary-layer processes on near-surface turbulence within the West African Monsoon, Bound.-Lay. Meteorol., 136, 1–23, 2010.
 - Lothon, M., Lenschow, D. H., Mayor, S. D.: Coherence and scale of vertical velocity in the convective boundary layer from a Doppler lidar, Bound.-Lay. Meteorol., 121, 521–536, 2006.

- Lundquist, J. K.: Intermittent and elliptical inertial oscillations in the atmospheric boundary layer, J. Atmos. Sci., 60, 2661–2673, 2003.
- Mahrt, L.: The early evening boundary layer transition, Q. J. Roy. Meteor. Soc., 107, 329–343, 1981.
- Mahrt, L.: Stratified atmospheric boundary layers, Bound.-Lay. Meteorol., 90, 375–396, 1999. Mahrt, L.: Stably stratified boundary layers, Annu. Rev. Fluid Mech., 46, 23–45, 2014.
 - Mahrt, L. and Lenschow, D. H.: Growth dynamics of the convectively mixed layer, J. Atmos. Sci., 33, 41–51, 1976.
 - Mahrt, L., Vickers, D., Nakamura, R., Soler, M. R., Sun, J., Burns, S., and Lenschow, D. H.: Shallow drainage flows, Bound.-Lay. Meteorol., 101, 243–260, 2001.
 - Manins, P. C. and Sawford, B. L.: Katabatic winds: a field case study, Q. J. Roy. Meteor. Soc., 105, 1011–1025, 1979.
 - Martin, S., Bange, J., and Beyrich, F.: Meteorological profiling of the lower troposphere using the research UAV "M²AV Carolo", Atmos. Meas. Tech., 4, 705–716, doi:10.5194/amt-4-705-2011, 2011.
 - McNaughton, K. G., Clement, R. J., and Moncrieff, J. B.: Scaling properties of velocity and temperature spectra above the surface friction layer in a convective atmospheric boundary layer, Nonlin. Processes Geophys., 14, 257–271, doi:10.5194/npg-14-257-2007, 2007.
- Moene, A. F., Beyrich, F. B., and Hartogensis, O. K.: Developments in scintillometry, B. Am. Meteorol. Soc., 90, 694–698, 2009.
- Moeng, C.-H.: A large-eddy-simulation model for the study of planetary boundary-layer turbulence, J. Atmos. Sci., 41, 2052–2062, 1984.
- Moeng, C.-H. and Sullivan, P. P.: A comparison of shear and buoyancy driven planetary-boundary-layer flows, J. Atmos. Sci., 51, 999–1022, 1994.
- Monin, A. S. and Obukhov, A. M.: Basic laws of turbulent mixing in the surface layer of the atmosphere, Tr. Akad. Nauk SSSR Geofiz., 24, 163–187, 1954.
 - Monin, A. S. and Yaglom, A. M.: Statistical Fluid Mechanics, Vol. 2, edited by: Lumley, J. L., The MIT Press, Massachusetts, 1975.
- Nadeau, D. F., Pardyjak, E. R., Higgins, C. W., Fernando, H. J. S., and Parlange, M. B.: A simple model for the afternoon and early evening decay of convective turbulence over different land surfaces, Bound.-Lay. Meteorol., 141, 301–324, 2011.
 - Nicoll, K. A. and Harrison, R. G.: Balloon-borne disposable radiometer for cloud detection, Rev. Sci. Instrum., 83, 025111, doi:10.1063/1.3685252, 2012.

- Nieuwstadt, F. T. M.: The turbulent structure of the stable, nocturnal boundary layer, J. Atmos. Sci., 41, 2202–2216, 1984.
- Nieuwstadt, F. T. M. and Brost, R. A.: The decay of convective turbulence, J. Atmos. Sci., 43, 532–546, 1986.
- Pardyjak, E. R. and Fernando, H. J. S.: The effect of surface type on the decay of turbulence in the surface layer during evening transition, in: Proc: 9th EMS Annual Meeting, 28 September–2 October 2009, Toulouse, France, 2009.
- Pielke, R. A.: Mesoscale Meteorological Modeling, 2nd edn., Academic Press, Amsterdam, 676 pp., 2002.
- Pietersen, H. P., Vilà-Guerau de Arellano, J., Augustin, P., de Coster, Durand, P., Gioli, B., Hartogensis, O., Lothon, M., Lohou, F., Pino, D., Ouwersloot, H. G., Reuder, J., and van de Boer, A.: Study of a prototypical convective boundary layer observed during BLLAST: contributions by large-scale forcing, Atmos. Chem. Phys. Discuss., in preparation, 2014.
- Pino, D., Jonker, H. J. J., Vilà-Guerau de Arellano, J., and Dosio, A.: Role of shear and the inversion strength during sunset turbulence over land: characteristic length scales, Bound.-Lay. Meteorol., 121, 537–556, 2006.
 - Pope, S. B.: Turbulent Flows, Cambridge University Press, Cambridge, 771 pp., 2000.
- Poulos, G. S., Blumen, W., Fritts, D. C., Lundquist, J. K., Sun, J., Burns, S., Nappo, C., Banta, R., Newsom, R., Cuxart, J., Terradellas, E., Balsley, B., and Jensen, M.: CASES-99: a comprehensive investigation of the stable nocturnal boundary layer, B. Am. Meteorol. Soc., 83, 555–581, 2002.
- Reuder, J., Ablinger, M., Agustsson, H., Brisset, P., Brynjolfsson, S., Garhammer, M., Johannesson, T., Jonassen, M., Kuehnel, R., Laemmlein, S., de Lange, T., Lindenberg, C., Malardel, S., Mayer, S., Mueller, M., Olafsson, H., Roegnvaldsson, O., Schaeper, W., Spengler, T., Zaengl, G., and Egger, J.: FLOHOF 2007: an overview of the mesoscale meteorological field campaign at Hofsjökull, Central Iceland, Meteorol. Atmos. Phys., 116, 1–13, 2012a.
- Reuder, J., Jonassen, M., and Olafsson, H.: The Small Unmanned Meteorological Observer SUMO: recent developments and applications of a Micro-UAS for atmospheric boundary layer research, Acta Geophys., 60, 1454–1473, 2012b.
- Rizza, U., Miglietta, M. M., Degrazia, G. A., Acevedo, O. C., and Marques, E. P.: Sunset decay of the convective turbulence with large-eddy simulation under realistic conditions, Physica A, 392, 4481–4490, 2013.

- Román-Cascón, C., Yagüe, C., Viana, S., Sastre, M., Maqueda, G. Lothon, M., and Gómara, I.: Near monochromatic ducted gravity waves associated with a convective system close to the Pyrénées, Q. J. Roy. Meteor. Soc., in review, 2014.
- Saïd, F., Corsmeier, U., Kalthoff, N., Kottmeier, C., Lothon, M., Wieser, A., Hofherr, I., and Pascal, P.: ESCOMPTE experiment: intercomparison of four aircraft dynamical, thermodynamical, radiation and chemical measurements, Atmos. Res., 74, 217–252, 2005.
- Sastre, M., Yagüe, C., Román-Cascón, C., Maqueda, G., Lothon, M., and Saïd, F.: Pressure perturbations and multi-scale analysis in the atmospheric boundary layer at the afternoon and evening transition during the BLLAST campaign, in: Proc. 20th Symposium on Boundary-Layers and Turbulence, 7–13 July, Boston, MA, USA, 2012.
- Sastre, M., Steeneveld, G.-J., Yagüe, C., Román-Cascón, C., and G. Maqueda: WRF tests on atmospheric boundary layer transitions during BLLAST campaign, Atmos. Chem. Phys. Discuss., in preparation, 2014.
- Seibert, P., Beyrich, F., Gryning, S.-E., Rasmussen, A., and Tercier, P.: Review and intercomparison of operational methods for the determination of the mixing height, Atmos. Environ., 34, 1001–1027, 2000.
 - Seity, Y., Brousseau, P., Malardel, S., Hello, G., Bénard, P., Bouttier, F., Lac, C., and Masson, V.: The AROME-France Convective-Scale Operational Model, Mon. Weather Rev., 139, 976–991, 2011.
- Shaw, W. J. and Barnard, J. C.: Scales of turbulence decay from observations and direct numerical simulations, in: Proc. of the 15th Symposium on Boundary Layers and Turbulence, 15–19 July 2002, Wageningen, the Netherlands, 2002.
 - Soler, M. R., Infante, C., Buenestado, P., and Mahrt, L.: Observations of nocturnal drainage flow in a shallow gully, Bound.-Lay. Meteorol., 105, 253–273, 2002.
- Sorbjan, Z.: Decay of convective turbulence revisited, Bound.-Lay. Meteorol., 82, 501–515, 1997.
 - Sorbjan, Z.: Gradient-based scales and similarity laws in the stable boundary layer, Q. J. Roy. Meteor. Soc., 136, 1243–1254, 2010.
 - Sorbjan, Z.: The height correction of similarity functions in the stable boundary layer, Bound.-Lay. Meteorol., 142, 21–31, 2012.
 - Steeneveld, G. J., Wokke, M. J. J., Groot Zwaaftink, C. D., Pijlman, S., Heusinkveld, B. G., Jacobs, A. F. G., and Holtslag, A. A. M.: Observations of the radiation divergence in the surface

- layer and its implication for its parameterization in numerical weather prediction models, J. Geophys. Res., 115, D06107, doi:10.1029/2009JD013074, 2010.
- Stensrud, D. J.: Parameterization Schemes, Cambridge University Press, 459 pp., 2007.
- Stull, R. B.: Energetics of entrainment across a density interface, J. Atmos. Sci., 33, 1260–1267, 1976.
- Stull, R. B.: An Introduction to Boundary Layer Meteorology, Kluwer Academic Press, Dordrecht, 688 pp., 1988.
- Sun, J., Burns, S. P., Delany, A. C., Oncley, S. P., Horst, T. W., and Lenschow, D. H.: Heat balance in the nocturnal boundary layer during CASES-99, J. Appl. Meteorol., 42, 1649–1666, 2003.
- Sun, J., Mahrt, L., Banta, R. M., and Pichugina, Y. L.: Turbulence regimes and turbulence intermittency in the stable boundary layer during CASES-99, J. Atmos. Sci., 69, 338–351, 2012.
- Svensson, G., Holtslag, a. a. M., Kumar, V., Mauritsen, T., Steeneveld, G. J., Angevine, W. M., Bazile, E., Beljaars, A., Bruijn, E. I. F., Cheng, A., Conangla, L., Cuxart, J., Ek, M., Falk, M. J., Freedman, F., Kitagawa, H., Larson, V. E., Lock, A., Mailhot, J., Masson, V., Park, S., Pleim, J., Söderberg, S., Weng, W., and Zampieri, M.: Evaluation of the diurnal cycle in the atmospheric boundary layer over land as represented by a variety of single-column models: the second GABLS experiment, Bound.-Lay. Meteorol., 140, 177–206, 2011.
- Tennekes, H. and Lumley, J. L.: A First Course in Turbulence, The MIT Press, Cambridge, Massachussets, 1973.
 - Van de Boer, A., Moene, A. F., Schuttemeyer, D., and Graf, A.: Sensitivity and uncertainty of analytical footprint models according to a combined natural tracer and ensemble approach, Agr. Forest Meteorol., 169, 1–11, 2013.
- Van Heerwaarden, C. C., Moene, A. F., and Holtslag, A. A. M.: Interactions between dry-air entrainment, surface evaporation and convective boundary-layer development, Q. J. Roy. Meteor. Soc., 135, 1277–1291, 2009.
 - Van den Kroonenberg, A. C., Martin, S., Beyrich, F., and Bange, J.: Spatially-averaged temperature structure parameter over a heterogeneous surface measured by an unmanned aerial vehicle, Bound.-Lay. Meteorol., 142, 55–77, 2012.
 - Van de Wiel, B. J. H., Ronda, R. J., Moene, A. F., De Bruin, H. A. R., and Holtslag, A. A. M.: Intermittent turbulence and oscillations in the stable boundary layer over land, Part I: A bulk model, J. Atmos. Sci., 59, 942–958, 2002a.

- Van de Wiel, B. J. H., Moene, A. F., Ronda, R. J., De Bruin, H. A. R., and Holtslag, A. A. M.: Intermittent turbulence and oscillations in the stable boundary layer over land, Part II: A system dynamics approach, J. Atmos. Sci., 59, 2567–2581, 2002b.
- Van de Wiel, B. J. H., Moene, A. F., Hartogensis, O. K., De Bruin, H. A. R., and Holtslag, A. A. M.: Intermittent turbulence in the stable boundary layer over land, Part III: A classification for observations during CASES-99, J. Atmos. Sci., 60, 2509–2522, 2003.
 - van Driel, R. and Jonker, H. J. J.: Convective boundary layers driven by nonstationary surface heat fluxes, J. Atmos. Sci., 68, 727–738, 2011.
- Van Ulden, A. P. and Wieringa, J.: Atmospheric boundary layer research at Cabauw, Bound.-Lay. Meteorol., 78, 39–69, 1996.
- Viana, S., Yagüe, C., and Maqueda, G.: Propagation and effects of a mesoscale gravity-wave over a weakly-stratified nocturnal boundary layer during SABLES2006 field campaign, Bound.-Lay. Meteorol., 133, 165–188, 2009.
- Viana, S., Terradellas, E., and Yagüe, C.: Analysis of gravity waves generated at the top of a drainage flow, J. Atmos. Sci., 67, 3949–3966, 2010.
 - Vilà-Guerau de Arellano, J., Dosio, A., Vinuesa, J.-F., Holtslag, a. a. M., and Galmarini, S.: The dispersion of chemically reactive species in the atmospheric boundary layer, Meteorol. Atmos. Phys., 87, 23–38, 2004.
- Vilà-Guerau de Arellano, J., van den Dries, K., and Pino, D.: On inferring isoprene emission surface flux from atmospheric boundary layer concentration measurements, Atmos. Chem. Phys., 9, 3629–3640, doi:10.5194/acp-9-3629-2009, 2009.
- Willis, G. E. and Deardorff, J. W.: A laboratory model of diffusion into the convective planetary boundary layer, Q. J. Roy. Meteor. Soc., 102, 427–445, 1976.
- Wyngaard, J. C.: Turbulence in the Atmosphere, Cambridge University Press, England, 393 pp., 2010.
 - Yagüe, C. and Cano, J.: Eddy transfer processes in the atmospheric boundary layer, Atmos. Environ., 28, 1275–1289, 1994.
 - Zhu, P. and Albrecht, B.: A theoretical and observational analysis on the formation of fair-weather cumuli, J. Atmos. Sci., 59, 1983–2005, 2002.

 Table 1. Groups involved in the BLLAST campaign and the instrumentation they implemented.

Country, group	Instrumentation
France, LA	Wind profilers, Surface station, Tethered balloon, Radiosounding
France, CNRM-GAME	Wind profiler, Lidar, ceilometer, scintillometer, Surface station, Turbulent probe under tethered balloon, Frequent Radiosounding
France, SAFIRE	Piper Aztec aircraft
France, LPCA	Sodar, Surface station, SMPS and cascade impactor
France, LMD	Lidar
the Netherlands, MAQ	Sodar, scintillometer, Surface station
USA, Utah Univ.	Surface station, tethered balloon
USA, UC Davis	Radiosoundings
Italy, CNR	Sky Arrow aircraft
Spain, Univ. Comp. de Madrid	Microbarometers
Spain, Universitat de les Illes Balears	Surface station, soil measurements
Norway, Univ. Bergen	SUMO RPAS, surface station
Germany, Univ. Tübingen	MASC RPAS
Germany, Univ. Braunschweig	M2AV RPAS
Germany, Univ. Lipp	Octo-copter RPAS
Germany, Univ. Heidelberg	Sirius I RPAS
Germany, Univ. Bremen	BUSCA RPAS, Funjet1 RPAS, Funjet2 RPAS
Switzerland, PMOD-WRC	Radiation sensors
UK, Univ. Reading	Sensors on SUMO RPAS

Table 2. Intensive observations made by the two aircraft (number of flights (FL) and hours), Remotely piloted aircraft system (RPAS) (number of flights), radiosoundings (RS) (number of launches), and tethered balloons (TB) (duration).

	AIRC	RAFT		RPAS		RS				TB
	Sky Arrow	Piper Aztec	SUMO	M2AV	Octo- copter	Site1	Site2	Site3	Site 1	Site 2 Moor/maize
IOP00 14 Jun 2011	2 FL (2 h)		3 FL			8	1			
IOP01 15 Jun 2011	2 FL (4 h)	2 FL (3 h)	21 FL			7	6		8 h	6 h/5 h
IOP02 19 Jun 2011	2 FL (4 h)	2 FL (4 h)	28 FL			4	8		8 h	6 h/4 h
IOP03 20 Jun 2011	3 FL (5 h)	2 FL (4 h)	23 FL			4	7		8 h	5 h/4 h
IOP04 24 Jun 2011	2 FL (4 h)		12 FL			4				
IOP05 25 Jun 2011	3 FL (4 h)	3 FL (5 h)	19 FL			4	8		8 h	3 h/7 h
IOP06 26 Jun 2011	2 FL (4 h)	2 FL (4 h)	23 FL			6	6	1	8 h	6 h/7 h
IOP07 27 Jun 2011	(2 h)	2 FL	35 FL			6	2	2	8 h	6 h/5 h
IOP08 30 Jun 2011		2 FL (4.5 h)	17 FL	2 FL		3			8 h	5 h/4 h
IOP09 1 Jul 2011		2 FL (4.5 h)	11 FL	2 FL	10 FL	7	8		8 h	7 h/7 h
IOP10 2 Jul 2011		2 FL (4 h)	12 FL	4 FL	8 FL	6	8		8 h	5 h/5 h
IOP11 5 Jul 2011		3 FL (6 h)	14 FL	5 FL	14 FL	8	8	3	8 h	6 h/4 h
Sub-Total	16 FL (27 h)	22 FL (41 h)	218 FL	13 FL	22 FL	67	62	6	80 h	55 h/50 h
Total		lights 8 h	2	60 flights	3	13	135 launches 18		185 h	

Table A1. Surface stations deployed during BLLAST: altitude, characteristics of the vegetation and measurements heights. The instruments used over each station are given in Table A2.

Site	Land use	Station Height (m a.s.l.)	Instrumentation Levels (m a.g.l.)
ss1	Wheat, rhye and peas Grass	582 581	0.5 to 5.8 0.5 to 5.8
	Wheat/grass edge	581	1 to 2.89
ss2	Grass	591 ± 5	0.1 to 8.22
ss3	Grass shrubs	601	0 to 9
ss4	Mixed (60 m tower)	602	2, 15, 30, 45, 60
ss5	Douglas Fir (20–25 m height)	620	21.8 to 31.5
ss6	Corn (0.4 to 1.5 m height)	645 ± 5	6
ss7	Moor	641 ± 3	2

Table A2. List of the variables measured at the surface sites (first column), instruments used (second column) and their acquisition frequency (third column). The abbreviation for the measured variables are T: temperature, WS: wind speed, WD: wind direction, H₂O: humidity, CO₂: carbon dioxide concentration, P: pressure, Rad: radiative budget terms, ST: soil temperature, SM: soil moisture, G: ground heat flux. For each surface station, the number of specific instruments installed is indicated (columns 4 to 12). Note that the lines in italic correspond to high frequency instruments.

	Instrument	Acq. Freq. (Hz)		ss1		ss2	ss3	ss4	ss5	ss6	ss7
			wheat	grass	edge					corn	mooi
T, H₂O	Campbell HMP45	0.1						5	1	1	1
T -	Campbell Thermocouple ASP TC	0.016					1				
T , H_2O	Psychrometer	0.1	5	5					l		
H ₂ O	Atexis PT1000 classe A	0.016								1	1
T	Campbell Thermocouple E-TYPE FW05	20				9					
WS	Vector Instrument A100LK	0.016					3				
WD	VectorInstrument W200P	0.016					3				
WS	Cup anemometer	0.1	5	5				1		l	
WD	Vane	0.1	1	1				1			
WS, WD	Young 05103	0.016						1	l	1	1
T, WS, WD	Campbell-scientific-CSAT-sonic-anemo	10-20	1	1	1	4	1	2	2		
WS, WD	Kaio Denki	10–20				2					
T, WS, WD	Gill master pro sonic anemometer	10						1	l	1	1
WD	USA-1 sonic	20					1				
H_2O , CO_2	Licor 7500A CO2/H2O analyzer	10	1	1	1			1	1	1	1
H ₂ O	Campbell KH20 hygrometer	10						1			
Р	Vaisala PTB210							1		1	1
P	Vaisala PTB100a		1	1	1						
P	Paroscientific microbarometers	2					3				
Rad	CNR1 Kipp & Zonen	1	1	1			1	1	1	1	1
Rad	Hukseflux IR02 radiometers	0.1				6					
Rain	Rain gauge ARG100	0.1						1			
Rain	SPIEA raingauge	0.016						1		1	1
ST	Custom-built Pt100	0.1	5	5						1	1
ST	Atexis PT 1000 Classe A	0.016								1	1
SM	Delta Devices THETA PROBE ML2X	0.001	1	1	1		30			1	1
G	Hukseflux HFP01	0.1	1 1	1		l	2	3	l .	3	l 3

 Table A3. Instrumentation of the Piper Aztec aircraft.

Parameters	Instruments	Accuracy	Acquisition/computation Frequency
Position (lat., long. & alt.)	GPS + Inertial Navigation System (IXSEA AIRINS)	5 m	1 Hz
3-D ground-speed		0.03ms^{-1}	100 Hz
Height above the ground	Radar altimeter till 2500ft	50 m	1 Hz
Attitude angles (roll, pitch & true heading)	IXSEA AIRINS	0.005°, 0.02° for heading	100 Hz
Horizontal wind	Gust probe + IXSEA AIRINS	2 m s ⁻¹	25 Hz
3-D turbulent wind		0.01 ms ⁻¹	
Static pressure	Rosemount 1221	0.2 hPa	200 Hz
Temperature	Rosemount 102E2 thermometer	0.5°C	200 Hz
Relative humidity	capacitive sensor (CORECI Humicor 5000)	≤ 5%	50 Hz
Dew point temperature	Buck Research 1011B	±0.5°C	25 Hz
H ₂ O concentration (fluctuation)	Licor 7500 open-path gaz analyser	0.003 g kg ⁻¹	10 Hz
CO ₂ concentration (fluctuation)		0.1 ppb	10 Hz

Table A4. Instrumentation of the Sky Arrow aircraft.

Parameters	instruments	Accuracy	Acquisition Frequency		
Position (lat, long & alt)	GPS (Novatel RT 20, single freq.) extended to 50 Hz with probe accelerometers	10 cm accuracy	10 Hz		
3-D ground speed		±1 cm s ⁻¹ accuracy	10 Hz		
Attitude angles (pitch, roll & true heading)	itude angles (pitch, roll & true heading) Systron Donner C-MIGITS III GPS-INS extended to 50 Hz with differential accelerometers		50 Hz		
3-D-wind (mean and turbulence)	Best Aircraft Turbulence (BAT) probe	Turbulence acc. $\pm 2\text{cm}\text{s}^{-1}$ mean wind acc. $\pm 0.5\text{m}\text{s}^{-1}$	50 Hz		
Humidity (abs. Humidity and dew point)	EdgeTech Model 200 Chilled Mirror	±0.5°C	50 Hz		
Temperature	Reference thermistor (mod YSI 4400) coupled to fast response thermocouple	±0.2°C	50 Hz		
Surface temperature	Everest 4000.4GL infrared radiometer	15° viewing angle, 8–14 µm, $\pm 0.5^{\circ}\text{C}$ accuracy	50 Hz		
Radiation	PAR up and down-welling (mod. Licor LI190) REBS Q*7 net radiometer	±5%	50 Hz		
CO ₂ concentration	Licor 7500 open-path gas analyzer	1 %	50 Hz		
H ₂ O concentration	Licor 7500 open-path gas analyzer	2%	50 Hz		

Table A5. RPAS which participated in the BLLAST field experiment. RPAS Weight, cruise velocity and measured variables are indicated. T, q, LST, Imagery, rad. and elec. stand for air temperature (°C), specific humidity (g kg⁻¹), land surface temperature (°C), downward shortwave radiation (W m⁻²), and electric charges, respectively. Note that the RPAS Syrius Busca, Funjet1 and Funjet2 do not appear in Table 2, as they did not fly during IOP days.

airframe	Reference	Weight	Acquisition frequency (Hz) of the measured variables						
		Cruise velocity	T & q	3-D-Wind	LST	imagery	rad.	elec.	
SUMO	Reuder et al. (2012b) Nicoll and Harrison (2012)	0.6 kg 54 kmh ⁻¹	2	100	2		10	10	
MASC	Van den Kroonenberg et al. (2012)	5 kg 90 km h ⁻¹	100	100					
M2AV	Martin et al. (2011)	6 kg 80 km h ⁻¹	100	100					
Octo-copter		1.7 kg 18 km h ⁻¹	50		50				
Sirius I		2.7 kg 65 km h ⁻¹	8		8	About 0.5–1*			
BUSCA		1.6 kg 60 km h ⁻¹	2						
Funjet1 Funjet2		0.7 kg 54 km h ⁻¹	2						

^{*} Triggered by autopilot to ensure 85 % image overlap.

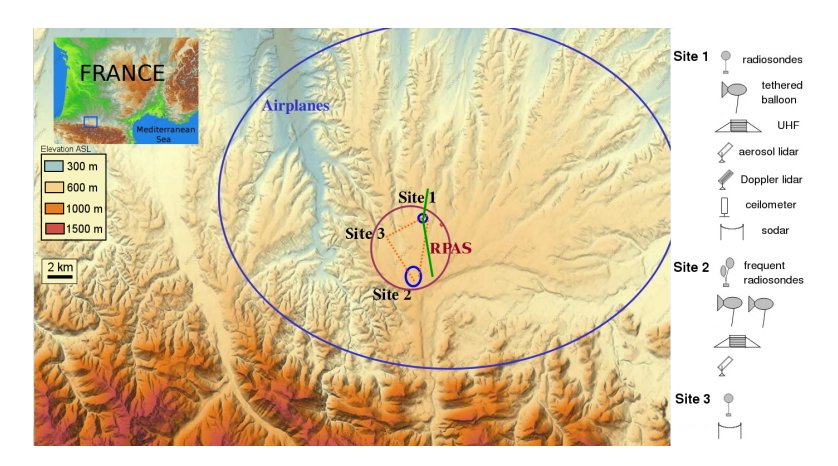


Fig. 1. Experimental area. The small frame at the top-left corner situates the BLLAST experiment area (blue square) at the larger scale of the country. The large blue oval delimits the exploration area of the manned aircraft, and the smaller purple circle indicates the Temporary Restricted Area (TRA) for the operations of the Remotely Piloted Aircraft Systems (RPAS). The orange dotted triangle locates the profiler network, and the green lines represent the paths of the two large aperture scintillometers. Instruments (other than surface stations) deployed over the three sites are schematized on the right side of the figure.

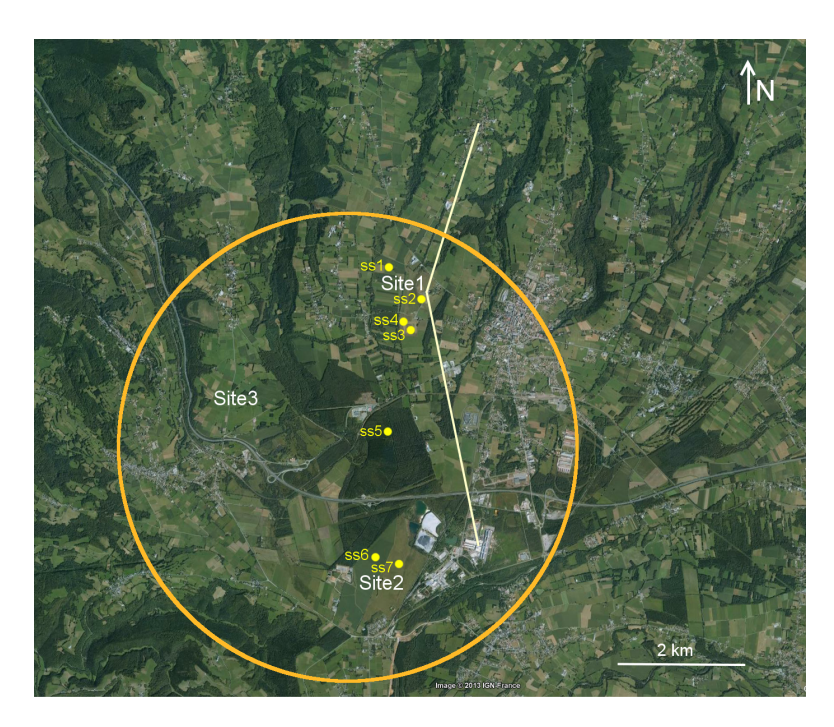


Fig. 2. Satellite view (from Google Earth) of the area, showing the instrumented site locations. Surface sites over various canopies are noted ss1 to ss7: (ss1) wheat, grass and edge, (ss2) prairies, (ss3) micro scale surface heterogeneities, (ss4) 60 m tower, (ss5) forest, (ss6) maize, and (ss7) moor. The yellow lines represent the paths of the two large aperture scintillometers and the orange circle indicates the limit of the TRA.

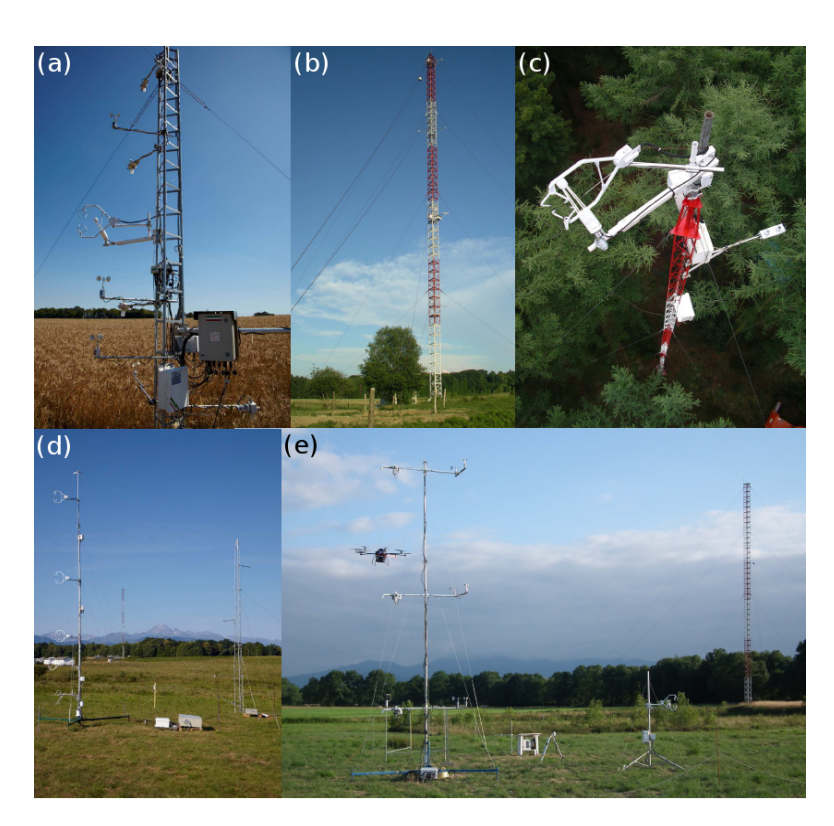


Fig. 3. Examples of surface sites during BLLAST: (a) one of the towers at the ss1 over the wheat, (b) ss4 with the 60 m tower, (c) ss5 over the forest, (d) ss2 over the prairies, and (e) ss3 over the micro scale heterogeneous surface with the ss4 60 m tower behind and the Octocopter flying around.

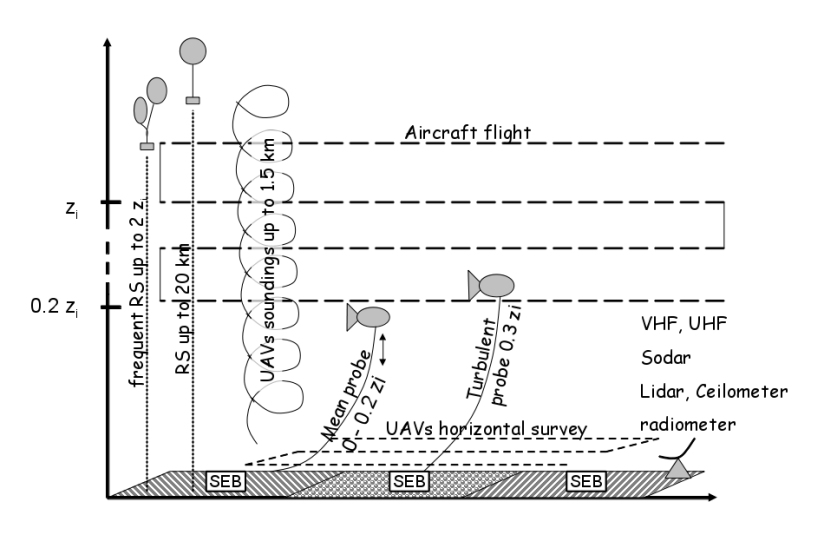


Fig. 4. Illustration of the observing strategy during the IOPs. RS = Radiosounding, RPAS = Remotely Piloted Aircraft System, SEB = Surface Energy Balance.

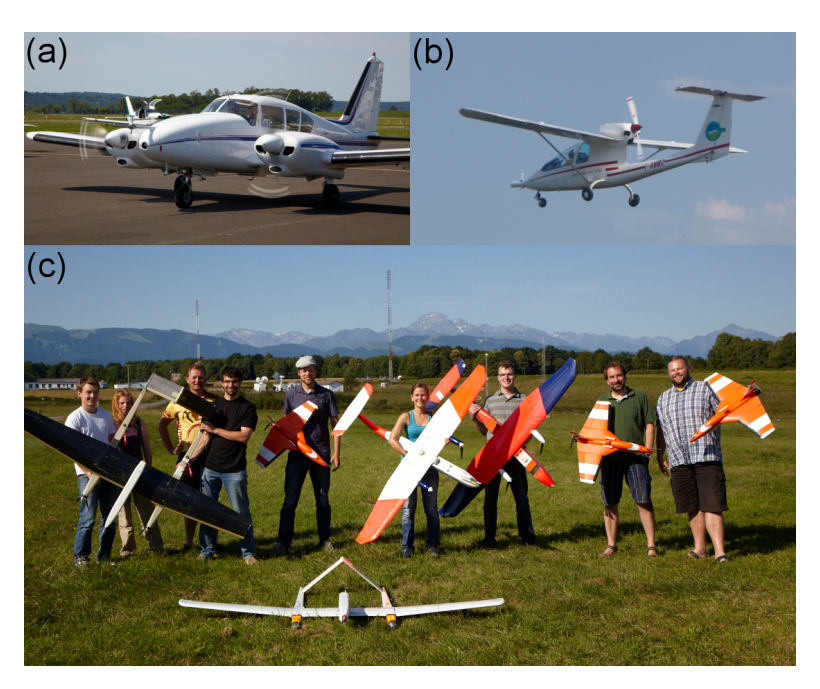


Fig. 5. (Top left) The SAFIRE Piper Aztec aircraft, (top right) the CNR Sky Arrow aircraft, and (bottom) the RPAS teams participating during most of the BLLAST campaign. The RPAS presented from left to right are: MASC (University of Tübingen, Germany), SUMO (University of Bergen, Norway), M2AV (2 planes, Technical University Braunschweig, Germany), SUMO (2 planes), and one MASC in front.

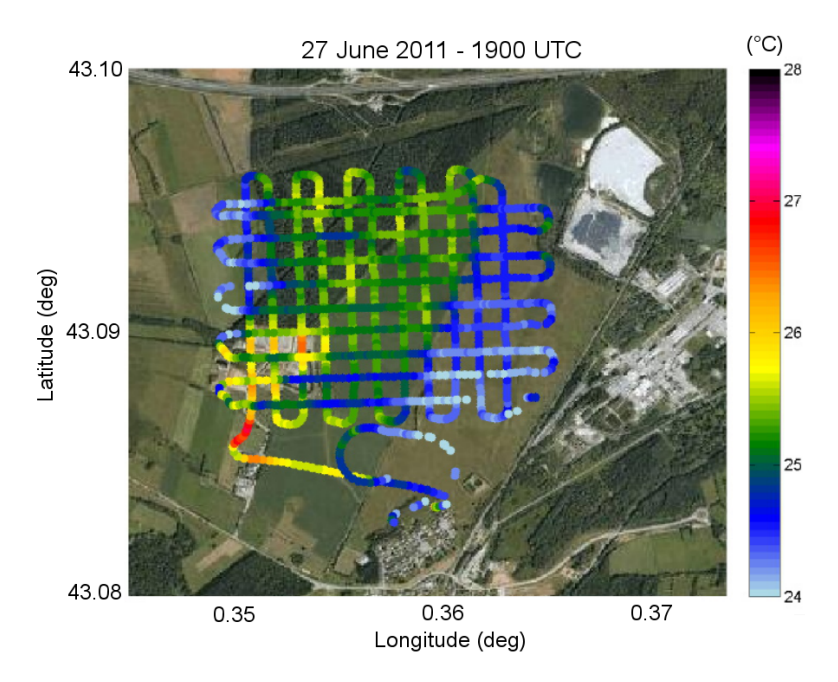


Fig. 6. Surface temperature observed by the RPAS SUMO during an exploration survey 60 m above ground at site 2 on 27 June 2011 (IOP 7). At that time and that day, the forest and the maize had similar temperatures, about 1 °C warmer than the moor. The hot spot on the bottom left is a bare ground and concrete surface of a waste disposal area (Google-bilder ©2011 COWI A/S, DDO, DigitalGlobe, GeoEye, Scankort @Google).

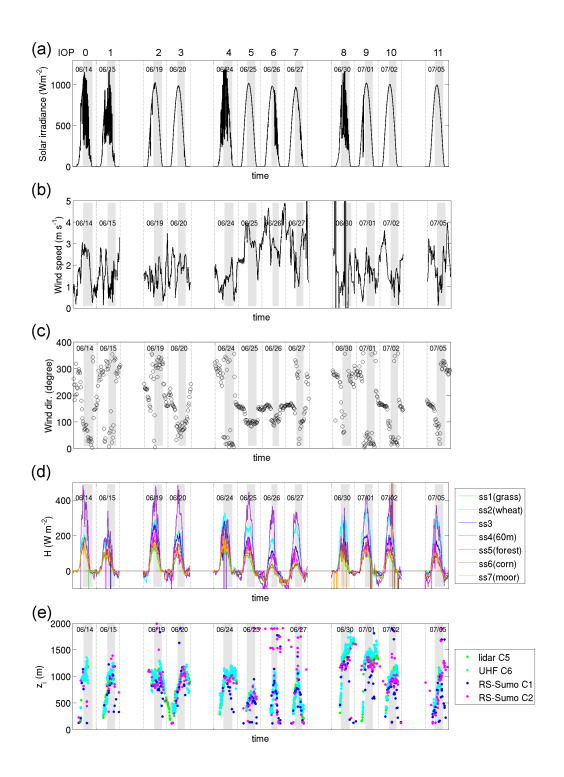


Fig. 7. Time series of (a) solar irradiance, (b) wind speed, (c) wind direction over the moor surface at site 2, (d) surface sensible heat flux H measured over several surfaces at the different sites (see Fig. 2) and (e) Estimates of Zi from various measurements, using criteria (C1) in dark blue, (C2) in pink, (C5) in green and (C6) in bright blue defined in the text. The shaded areas mark the AT period.



Discussion Paper

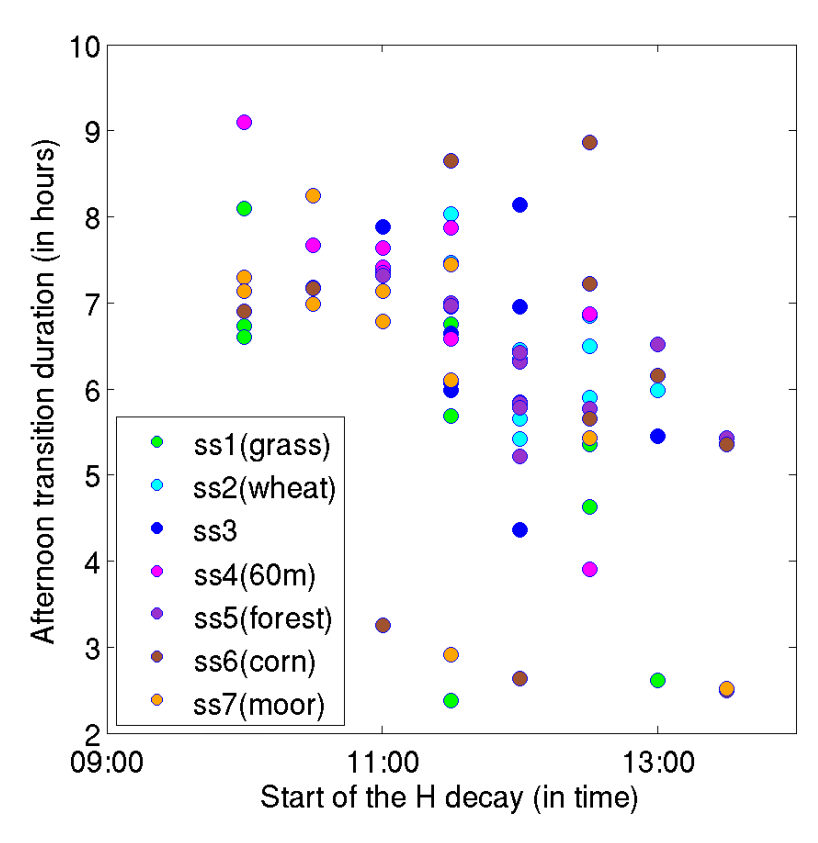


Fig. 8. Duration of the afternoon transition as a function of the starting time of the sensible heat flux decay over several surfaces and for all IOP days and sites (colors).

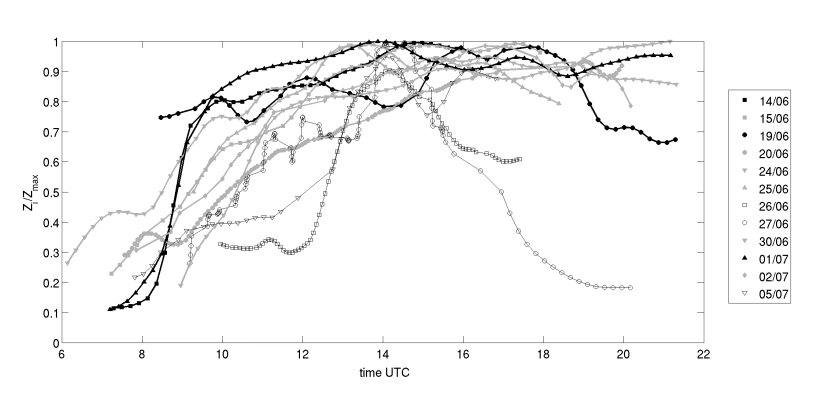


Fig. 9. Evolution of the CBL top, defined here as height of the top inversion Z_i , for all IOPs. Z_i is divided by the maximum height reached the same day for day-to-day comparison, and has been smoothed with a 1 h moving average. The estimates are made from lidar backscatter at site 1, except for day 26 June when the UHF radar estimates were used instead, due to missing data. One symbol is used per IOP. Three sets of cases have been identified: (thick black lines) rapid growth and levelling inversion in late afternoon, (thick grey lines) more typical growth and levelling inversion and (thin black lines) slower growth and rapidly decreasing top-inversion in late afternoon.



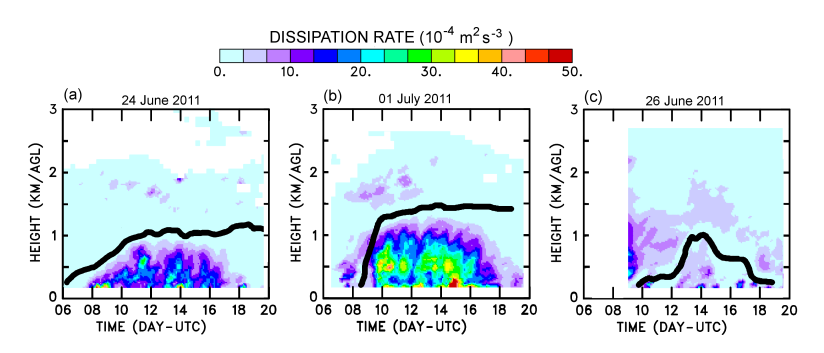


Fig. 10. Time-height section of TKE dissipation rate estimated from UHF wind profiler during (a) 24 June, (b) 1 July 2011 and (c) 26 June 2011. The evolution of the CBL top inversion (deduced from local maximum of the refractive index structure parameter) is indicated by the black thick line.

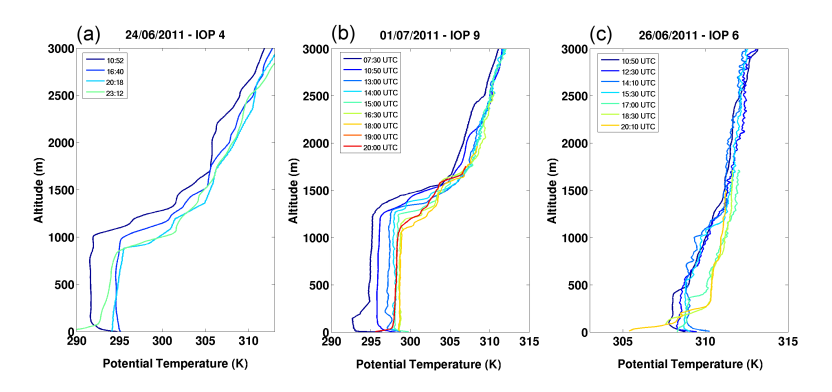


Fig. 11. Vertical profiles of potential temperature measured by radiosondes on (a) 24 June, (b) 1 July and (c) 26 June. The launching time is indicated in the top-left corner of each panel.

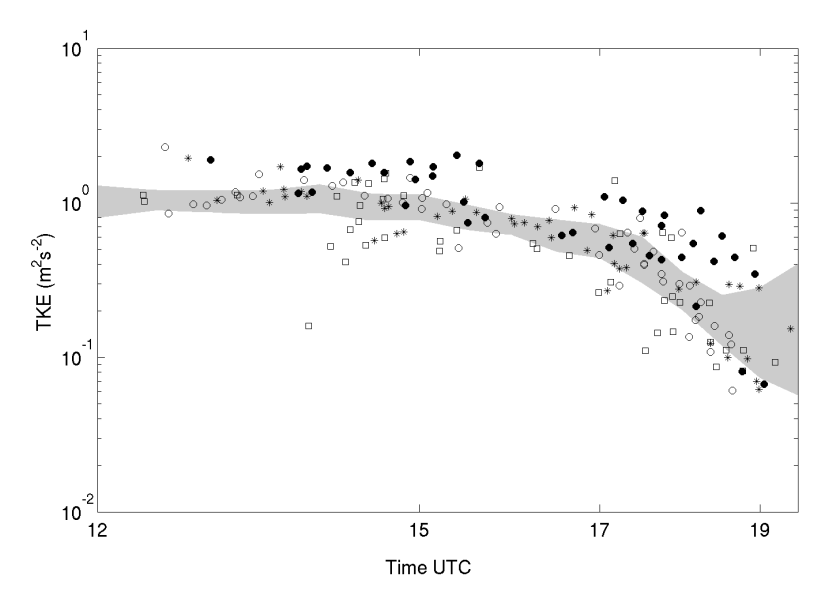


Fig. 12. TKE decay observed during all IOP days (shaded area) over 5 different surfaces and (symbols) from the legs flown by the Piper Aztec and Sky arrow aircraft. Note that a logarithmic scale is used on the y-axis. The shaded area represents the quantiles from 25 % to 75 % of surface estimates. The symbols for the airplane legs differ according to altitude: (closed circles) lowest quarter of the mixed or residual PBL ($Z < 0.25Z_i$), (asterisks) $0.25Z_i < Z < 0.5Z_i$, (open squares) $0.5Z_i < Z < 0.75Z_i$, (open circles) highest quarter ($0.75Z_i < Z < Z_i$).

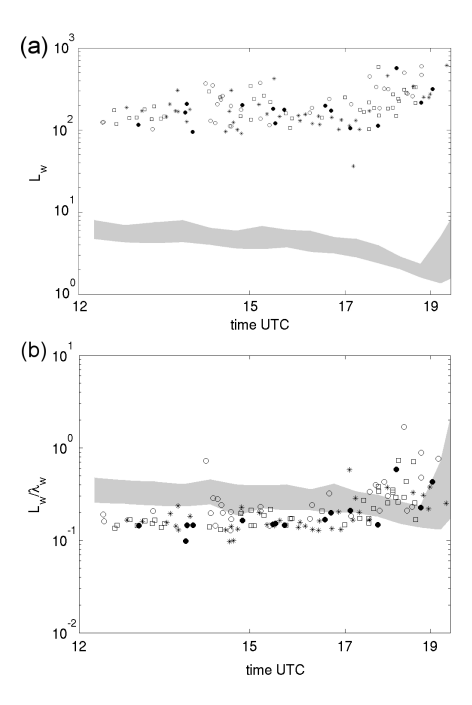


Fig. 13. Time evolution of **(a)** the air vertical velocity integral scales and **(b)** the ratio of the integral scales to the wavelength of maximum spectral energy during all IOP days. The shaded area represents the quartiles from 25 % to 75 % of ground-level estimates over 4 different surfaces and the symbols are used for legs flown at various heights by the Piper Aztec aircraft. The symbols for the airplane legs differ according to altitude: (closed circles) lowest quarter of the mixed or residual PBL ($Z < 0.25Z_i$), (asterisks) $0.25Z_i < Z < 0.5Z_i$, (open squares) $0.5Z_i < Z < 0.75Z_i$, (open circles) highest quarter $(0.75Z_i < Z < Z_i)$.